The Astrophysical Journal, 993:45 (18pp), 2025 November 1 https://doi.org/10.3847/1538-4357/adff75

Optical Spectroscopy Reveals Hidden Neutron-capture Elemental Abundance Differences among APOGEE-identified Chemical Doppelgängers*

Catherine Manea[1,13], Melissa Ness[2], Keith Hawkins[3], Greg Zeimann[4,5], David W. Hogg[6,7,8], Carrie Filion[8], Emily J. Griffith[9,13], Kathryn Johnston[1], Andrew Casey[8,10,11], Zoe Hackshaw[3], Tyler Nelson[12], and Micah Marks[3]
[1] Columbia Astrophysics Laboratory, Columbia University, New York, NY 10027, USA
[2] Research School of Astronomy and Astrophysics, Australian National University, Canberra, ACT 2601, Australia
[3] Department of Astronomy, The University of Texas at Austin, Austin, TX 78712, USA
[4] Hobby-Eberly Telescope, University of Texas at Austin, Austin, TX 78712, USA
[5] McDonald Observatory, The University of Texas at Austin, Austin, TX 78712, USA
[6] Center for Cosmology and Particle Physics, Department of Physics, New York University, 726 Broadway, New York, NY 10003, USA
[7] Max-Planck-Institut für Astronomie, Königstuhl 17, D-69117 Heidelberg, Germany
[8] Center for Computational Astrophysics, Flatiron Institute, 162 Fifth Avenue, New York, NY 10010, USA
[9] Center for Astrophysics and Space Astronomy, Department of Astrophysical and Planetary Sciences, University of Colorado, 389 UCB, Boulder, CO 80309-0389, USA
[10] School of Physics and Astronomy, Monash University, Melbourne, VIC 3800, Australia
[11] ARC Centre of Excellence for All Sky Astrophysics in Three Dimensions (ASTRO-3D), Australia
[12] Department of Physics, University of Southern Maine, Portland, ME 04104, USA
Received 2025 June 30; revised 2025 August 13; accepted 2025 August 17; published 2025 October 23

Abstract

Grouping stars by chemical similarity has the potential to reveal the Milky Way's evolutionary history. The APOGEE stellar spectroscopic survey has the resolution and sensitivity for this task. However, APOGEE lacks access to strong lines of neutron-capture elements ($Z > 28$), which have nucleosynthetic origins that are distinct from those of the lighter elements. We assess whether APOGEE abundances are sufficient for selecting chemically similar disk stars by identifying 25 pairs of chemical "doppelgängers" in APOGEE DR17 and following them up with the Tull spectrograph, an optical, $R \sim 60{,}000$ echelle on the McDonald Observatory 2.7 m telescope. Line-by-line differential analyses of pairs' optical spectra reveal neutron-capture (Y, Zr, Ba, La, Ce, Nd, and Eu) elemental abundance differences of Δ[X/Fe] $\sim 0.020 \pm 0.015$ to 0.380 ± 0.15 dex (4%–140%), and up to 0.05 dex (12%) on average, a factor of 1–2 times higher than intracluster pairs. This is despite the pairs sharing nearly identical APOGEE-reported abundances and [C/N] ratios, a tracer of giant-star age. This work illustrates that even when APOGEE abundances derived from spectra with a signal-to-noise ratio > 300 are available, optically measured neutron-capture element abundances contain critical information about composition similarity. These results hold implications for the chemical dimensionality of the disk, mixing within the interstellar medium, and chemical tagging with the neutron-capture elements.

Unified Astronomy Thesaurus concepts: S-process (1419); Surveys (1671); Chemical abundances (224); Galaxy chemical evolution (580)

Materials only available in the online version of record: machine-readable tables

1. Introduction

The chemical composition of some volume of the Galactic interstellar medium (ISM) is set by the legacy of chemical enrichment events (e.g., stellar nucleosynthesis and feedback, mixing, and accretion) that came prior. Stars form from the ISM and, in the absence of internal evolutionary processes such as dredge up and atomic diffusion, their surface compositions generally reflect the composition of the ISM from which they formed. Even as the surrounding ISM continues to evolve, stars retain a chemical memory of their birth environment, making them powerful tools for studying the Milky Way's fundamental processes. Spectroscopic surveys, such as Apache Point Observatory Galactic Evolution Experiment (APOGEE; e.g., Abdurro'uf et al. 2022), GALactic Archaeology with HERMES (GALAH; e.g., S. Buder et al. 2018, 2021), Gaia-ESO (e.g.,G. Gilmore et al. 2022; S. Randich et al. 2022), and Large Sky Area Multi-Object Fiber Spectroscopic Telescope Medium Resolution Survey (LAMOST MRS; e.g., C. Liu et al. 2020), are collecting a combined millions of medium-resolution ($R \sim 7500$ to $R \sim 28{,}000$ depending on the survey) stellar spectra that contain chemical information for up to 30 elements. With such a large quantity of chemical data, we are well-poised to explore chemical trends in the Galaxy in order to probe its star formation history, past accretion events, mixing mechanisms, and stellar nucleosynthesis.

Grouping stars by chemical similarity is fundamental to many Galactic studies that leverage stellar abundances to disentangle our Milky Way's evolutionary history and present day structure. For example, the seminal works of, e.g., N. G. Roman (1952), G. Wallerstein (1962), and B. M. Tinsley (1968, 1979) led to the discovery of a chemical bimodality in the Galactic disk where stars can be grouped into high and low α (e.g., O, Mg, Ca, and Si)

* This paper includes data taken with the Harlan J. Smith 2.7 m telescope at The McDonald Observatory of The University of Texas at Austin.
[13] NSF Astronomy and Astrophysics Postdoctoral Fellow.

populations (e.g., R. Gratton et al. 1996; K. Fuhrmann 1998; B. E. Reddy et al. 2003; T. Bensby et al. 2011; J. Bovy et al. 2012; F. Anders et al. 2014; M. R. Hayden et al. 2015; T. Buck 2020; J. Imig et al. 2023). Stellar abundances also aided in the discovery of the Gaia-Sausage-Enceladus system, a population of accreted stars in the inner Galactic halo that show distinct compositions (low Fe and low α among other chemical trends) and is understood to be the last major merger experienced by our Galaxy (e.g., V. Belokurov et al. 2018; C. R. Hayes et al. 2018; M. Haywood et al. 2018; A. Helmi et al. 2018; F. Vincenzo et al. 2019; A. Carrillo et al. 2022, 2024; I. Ciucă et al. 2024). The limit to which we can meaningfully group stars using chemistry alone has been a major question in the field in the last two decades. Understanding these limits in the disk is particularly important, as it harbors the outcome of in situ star formation. One potential limiting case is the separation of disk stars into their natal birth groups using chemistry alone (e.g., K. Freeman & J. Bland-Hawthorn 2002; J. Bland-Hawthorn et al. 2010), a method called strong chemical tagging. Even in the limit of negligible uncertainties, strong chemical tagging relies on (i) individual birth sites having unique mean chemical abundance vectors and (ii) intracluster abundance scatter that is small enough to be sufficiently discriminatory between clusters. While the literature agrees that stars in open clusters are generally highly chemically homogeneous (e.g., J. Bovy et al. 2016; M. Ness et al. 2018; V. J. Poovelil et al. 2020; J. Kos et al. 2021; A. Sinha et al. 2024—with some exceptions due to stellar evolution effects; e.g., F. Liu et al. 2016; D. Souto et al. 2018, 2019), open clusters at fixed age and birth radius tend to overlap in chemical composition (e.g., L. Casamiquela et al. 2021; L. Spina et al. 2022; A. Sinha et al. 2024). This is supported by, e.g., M. Ness et al.(2018), D. de Mijolla et al. (2021), and C. Manea et al.(2023), which found that the so-called chemical doppelgänger rate, the rate at which random pairs of field disk stars are as chemically similar as pairs of intracluster stars, is too high for strong chemical tagging to be feasible. As such, recent efforts have scaled back and instead focused on chemically grouping disk stars by similarity in Galactic birth radius and age or dynamical behavior. For example, M. K. Ness et al. (2019) found that [Fe/H] abundance and stellar age are enough to predict within 0.02 dex the chemical profile and orbit of an APOGEE DR14 (S. R. Majewski et al. 2017) low α-disk star. This result suggests that [Fe/H] and age alone are sufficient for finding stars with shared chemodynamical behaviors and thus Galactic origins in the low alpha disk. Numerous other works group stars by chemical similarity to study the Galactic disk (e.g., N. Price-Jones et al. 2020; W. X. Sun et al. 2020; C. M. Cheng et al. 2021; P. Re Fiorentin et al. 2021; A. M. Price-Whelan et al. 2021; D. K. Feuillet et al. 2022; J. Lian et al. 2022; M. Ortigoza-Urdaneta et al. 2023; D. Horta et al. 2024; S. Foster et al. 2024).

Separating stars into chemically similar populations is evidently an important tool for Galactic science. However, more commonly than not, the elements considered in such studies are restricted to the light (e.g., C, N), α (e.g., O, Mg, Ca, Si), odd-Z (e.g., Na, Al, Mn), and iron-peak (e.g., Fe, Ni, Cr) elements. Elements primarily produced by the neutron-capture process (i.e., atomic number $>$ 28) are paid comparatively less attention in this context because their lines are often weak and blended (especially in metal-rich stars) and thus difficult to measure. Additionally, most neutron-capture lines lie at blue wavelengths ($\lambda < 5500$ Å), a wavelength regime at which many detectors are insensitive and that some spectroscopic surveys do not access. APOGEE, for example, is an infrared (H band) survey that is often used for large scale Galactic disk studies due to its broad sampling of the disk and generally high abundance precision. However, APOGEE's wavelength coverage limits the survey to few, weak neutron-capture lines (e.g., Ce, Nd, Rb, and Yb; S. Hasselquist et al. 2016; K. Cunha et al. 2017) that are typically measured imprecisely, though the Brussels Automatic Code for Characterizing High accUracy Spectra (BACCHUS) Analysis of Weak Lines in APOGEE Spectra Survey (BAWLAS; C. R. Hayes et al. 2022) has improved our understanding of neutron-capture lines in APOGEE through empirical upper limits, among other things. By omitting neutron-capture elements from abundance-based studies of the disk, we may be missing information that is only captured by these elements.

It has been established that the neutron-capture elements behave differently in the disk relative to the lighter elements due to their unique production and dispersal timescales and mechanisms (e.g., E. J. Griffith et al. 2022, 2024). Asymptotic giant branch (AGB) stars produce half of the trans-iron ($Z > 28$) elements via the slow neutron-capture process (s-process) and release them into the ISM via stellar winds (e.g., A. I. Karakas & J. C. Lattanzio 2014). Stellar s-process abundance ratios show a strong correlation with stellar age (e.g., J. Simmerer et al. 2004; P. E. Nissen 2015; J. Carbajo-Hijarrubia et al. 2024; S. Vitali et al. 2024, and references throughout this manuscript). Additionally, some simulations suggest that s-process elements produced in AGB stars are dispersed and mixed across smaller volumes in the ISM relative to the remaining elements, which are produced in explosive sources (e.g., Y. Feng & M. R. Krumholz 2014; L. Armillotta et al. 2018; M. R. Krumholz & Y.-S. Ting 2018; A. Emerick et al. 2020). Their localized dispersal could therefore lead their abundances to vary more significantly between stars born within some fixed volume and time. Recent simulations by C. Zhang et al. (2025), however, suggest the opposite, highlighting that the mixing of neutron-capture elements within the ISM is still an open question. Extreme explosive events such as neutron-star mergers and hypernovae produce the remaining trans-iron elements via the rapid neutron-capture process (r-process; e.g., C. Kobayashi et al. 2020), and these elements may also show greater star-to-star variations across the disk as they are synthesized in events that are rare but highly productive (e.g., B. Côté et al. 2017; A. Recio-Blanco et al. 2021). Owing to their unique production sites and dispersal mechanisms, s- and r-process elements might provide additional tracer information about a star's Galactic origin beyond what is captured by the lighter ($Z < 28$) elements. By omitting these elements, studies may miss additional chemical information that would distinguish otherwise chemically similar stars. It is critical that we understand whether these elements are important when grouping stars by chemical similarity. Doing so also informs models of Galactic chemical evolution, neutron-capture nucleosynthesis, and mixing within the ISM.

In this work, we observe and analyze the optical spectra of a set of carefully selected stars to examine the behavior of neutron-capture elements in otherwise chemically similar stars. We identify chemically similar stars among a high

Table 1
Summary of Our Observations

Gaia DR3 Source ID	Name	ObsDate (YYYYMMDD)	Exp (s)	N_{exp}
604923367432823808	M67 a	20240119	1800	2
604920202039656064	M67 b	20240119	1800	2
604919480485158784	M67 c	20240119	1800	3
…	…	…	…	…
1509031094389703680	Pair47 a	20230530	1800	3
1332869540410728448	Pair47 b	20230529	1800	2
1393189710382298496	Pair49 a	20230531	1800	2
2106262308540128000	Pair49 b	20230531	1800	2
1313275448633710080	Pair50 a	20230529	1200	1
1414698013247715840	Pair50 b	20230529	1800	3
1489165668053970176	Pair52 a	20230613	1800	2
1201468623762697856	Pair52 b	20230613	1800	4
2593796720752077568	Pair6 a	20240119	1800	1
173154016016909568	Pair6 b	20240119	1800	6

(This table is available in its entirety in machine-readable form in the online article.)

signal-to-noise ratio (SNR; SNR $>$ 300) subset of APOGEE DR17 and assess their neutron-capture element similarity via high-resolution ($R \sim 60{,}000$), high-SNR (SNR $>$ 100) optical spectroscopic follow-up. We perform a high-precision, line-by-line differential analysis (see Section 3) to determine compositions in the lighter elements accessible by APOGEE as well as Cu, Zn, and seven neutron-capture elements (Y, Zr, Ba, La, Ce, Nd, and Eu) inaccessible to or imprecisely measured by APOGEE. We then address the following questions:

1. Are APOGEE-identified chemically similar stars also similar in the neutron-capture elements?
2. Why do some, if any, APOGEE-identified chemically similar stars differ in the neutron-capture elements despite possessing otherwise highly similar lighter ($Z < 29$) elemental abundances?
3. Does similarity in APOGEE-determined [Ce/Fe] correlate to similarity in optically measured [Ce/Fe]?

In addressing these questions, we explore whether APOGEE-measured elements are sufficient for finding chemically similar stars (e.g., M. K. Ness et al. 2019) or if neutron-capture elements may provide additional information to better identify stars with similar Galactic origins. This work informs future studies that rely on grouping stars by chemical similarity. Furthermore, our results provide an empirical constraint on the spatial and temporal complexity with which neutron-capture elements are synthesized, dispersed, and mixed across the ISM.

This manuscript is organized as follows. In Section 2, we describe the acquisition and reduction of high-resolution optical spectra of APOGEE DR17-identified chemically similar stars. In Section 3, we describe our method for determining the chemical similarity of these stars via high-precision, line-by-line differential analysis performed on the optical spectra. In Section 4, we present our results reporting the chemical similarity of the APOGEE-identified chemically similar pairs in both lighter ($Z < 29$) and heavier elements. In Section 5, we place our results in the context of past observational and theoretical works. Additionally, we compare our abundances to those reported by APOGEE and BAWLAS. We conclude with a summary in Section 6.

Table 2
List of Absorption Lines Used for Abundance Determination

Element	Ion	Central Wavelength (Å)
Na	1	4751.8
Ti	1	4758.1
Ti	1	4759.3
Ce	2	4773.9
…	…	…
Fe	1	5364.9
Fe	1	5365.4
Ti	1	5366.6
Fe	1	5379.6
Fe	1	5383.4
…	…	…
Fe	1	8621.6
Al	1	8773.9
Ti	1	8778.7
Fe	1	8846.7

Note. BACCHUS determines abundances with line-by-line spectral synthesis. As such, the above central wavelengths describe the center of the spectral window used in line-by-line abundance determination. Atomic data for the synthesis of each window are adopted from version 5 of the Gaia-ESO linelist. This list encompasses all possible spectral regions considered for abundance determination, though the specific subset of regions used for each star varies depending on individual spectral quality.

(This table is available in its entirety in machine-readable form in the online article.)

2. Data

2.1. Selection of APOGEE Chemical Doppelgängers for Optical Follow-up

In this work, we ask whether APOGEE-identified chemically similar stars are also similar when studied in the optical. Thus, we must first identify chemically similar stars in the APOGEE survey. The definition of chemical similarity is ambiguous, particularly when considering the ensemble of elemental abundances available in APOGEE, each of which are measured at different precisions. We adopt the definition of M. Ness et al. (2018, hereafter N18), which defines chemically similar stars to be pairs of stars that are just as chemically similar as those born together in the same molecular cloud. Field stars that match this description but show no kinematic indication of having formed together are called "chemical doppelgängers." N18's primary goal is to measure the chemical doppelgänger rate in APOGEE. To do this, they consider 20 elemental abundance ratios ([Fe/H], [C/Fe], [N/Fe], [O/Fe], [Na/Fe], [Mg/Fe], [Al/Fe], [Si/Fe], [S/Fe], [K/Fe], [Ca/Fe], [Ti/Fe], [V/Fe], [Mn/Fe], [Ni/Fe], [P/Fe], [Cr/Fe], [Co/Fe], [Cu/Fe], and [Rb/Fe]) homogeneously derived from APOGEE DR13 spectra using *The Cannon* (M. Ness et al. 2015). They draw random pairs of stars from the field unassociated with known open clusters and moving groups and quantify their abundance similarity using a χ^2 value defined as:

$$\chi^2_{nn'} = \sum_{i=1}^{I} \frac{[x_{ni} - x_{n'i}]^2}{\sigma^2_{ni} + \sigma^2_{n'i}}, \quad (1)$$

where the two stars in a pair are indexed as n, n', and x, σ are their derived abundance and abundance uncertainty in element i, respectively. This leads to a global chemical similarity metric for each stellar pair that considers all 20 elements. Chemical doppelgängers are defined as stellar pairs with χ^2

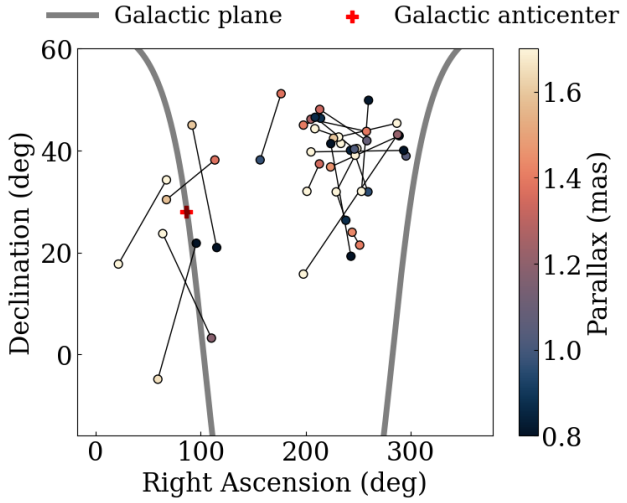

Figure 1. The R.A. vs. decl. distribution of our observed sample of APOGEE-identified doppelgängers. Doppelgängers are connected with a line and colored by their Gaia DR3 parallax. The Galactic plane is marked in gray, and the Galactic anticenter is marked by a red plus. Doppelgängers span a range of on-sky positions, parallaxes, and on-sky separations and do not appear to be kinematically related.

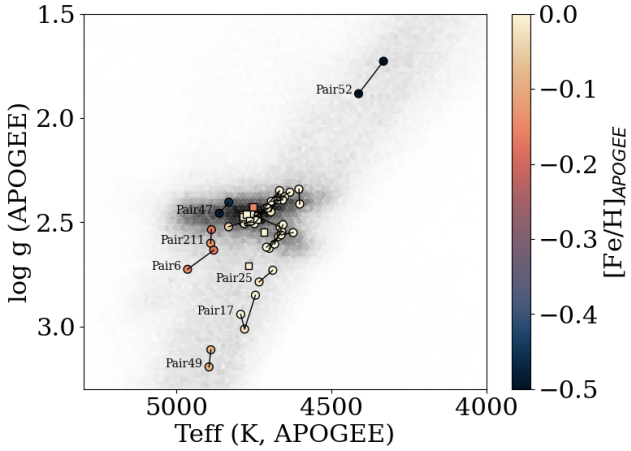

Figure 2. A Kiel diagram of our sample. Doppelgängers are represented by circles connected with a line and colored by APOGEE DR17-reported [Fe/H]. Squares represent the observed reference M67 stars. The background presents field stars from the APOGEE DR17 survey colored by number density. Pairs that lie at the edges of the distribution are labeled for interest. Doppelgängers span the red giant branch with the majority occupying the red clump. They display a range of metallicities, though the majority of doppelgängers have approximately solar [Fe/H].

values less than the median χ^2 value returned by random pairs of stars drawn from the same open cluster.

We generally follow the N18 method to find chemical doppelgängers for follow-up, though we deviate slightly from their approach. First, we work with APOGEE DR17 (Abdurro'uf et al. 2022) data, whereas N18 used DR13 data. Unlike N18, we do not re-derive APOGEE DR17 abundances using *The Cannon* (M. Ness et al. 2015) and instead work directly with the publicly released DR17 ASPCAP abundances. Our quality cuts are stricter to ensure that we only work with high-fidelity abundances: we only consider stars with SNR $>$ 300, 3650 $<$ TEFF $<$ 5760, 0.45 $<$ LOGG $<$ 3.95, FE_H_FLAG $=$ 0, X_FE_FLAG $=$ 0, and RUWE $<$ 1.4 (to avoid stars in binaries; e.g., V. Belokurov et al. 2020). When drawing stellar pairs, we require the stars to share $T_{\rm eff}$ within 50 K and log g within 0.1 dex. We consider the same elements as N18 with the exception of [P/Fe], [Cu/Fe], and [Rb/Fe], because few DR17 stars have unflagged abundances in these elements, and including these elements makes our sample size prohibitively small. However, unlike N18, we have access to APOGEE DR17-reported Ce, an *s*-process element, so we include it in our selection to test the efficacy of APOGEE's Ce at identifying stars with similar *s*-process elemental abundances. We highlight that we also include C and N in our selection of doppelgängers. Because C/N can trace stellar age in red giants (e.g., G. Casali et al. 2019; T. Spoo et al. 2022), including these elements in our selection increases the likelihood that doppelgängers are also similar in age.

As in N18, when searching for chemical doppelgängers, we ensure that we are selecting from the field as opposed to known clusters. To separate APOGEE DR17 into field and cluster stars, we use the open cluster membership catalog of T. Cantat-Gaudin et al. (2018, hereafter CG18). We consider field stars to be stars that do not exist in the CG18 catalog, and we consider open cluster stars to be stars in the CG18 catalog with a cluster membership probability exceeding 99%. This leaves us with 164 open cluster stars and 64,650 field stars. We then draw 3 million random pairs of stars from our high-fidelity field sample and compute χ^2 values for each pair using Equation (1). This process is repeated for all possible intracluster (within the same cluster) pairs from open clusters M67 and NGC 6819 (as in N18) to serve as our reference sample representing the chemical homogeneity of stars born together. Finally, as in N18, we draw and compute χ^2 values for all intercluster (across all clusters) pairs among the CG18 clusters. As in N18, we define doppelgängers to be field pairs with χ^2 less than or equal to the median χ^2 value for intracluster pairs. This analysis produces a pool of APOGEE chemical doppelgängers from which we can select targets. Final targets for optical follow-up were selected semirandomly from this pool, prioritizing bright ($V < 11$) stars to increase data acquisition efficiency.

In addition to following up APOGEE-identified chemical doppelgängers, we also target 11 giant stars in M67, an open cluster that has been found to be chemically homogeneous within abundance uncertainties when studying its giant stars (e.g., J. Bovy 2016; D. Souto et al. 2018; V. J. Poovelil et al. 2020; A. Sinha et al. 2024). These cluster stars will serve as a reference for the chemical homogeneity of conatal stars. We select stars from M67 with CG18-assigned membership probabilities >99% that have APOGEE DR17 spectra with SNR $>$ 100.[14] We are not able to observe NGC 6819, the second cluster used in N18, because its giant stars exceed the magnitude limit of the Tull spectrograph on the 2.7 m telescope.

2.2. Optical Spectra from the Tull Coudé Spectrograph on the McDonald Observatory 2.7 m Telescope

We obtained optical (3500 Å $<\lambda<$ 10,000 Å), high-resolution ($R \sim$ 60,000) spectra of 25 APOGEE doppelgängers and 11 M67 giant stars with the Tull Coudé Spectrograph on the McDonald Observatory 2.7 m telescope using Slit 4 (R. G. Tull et al. 1995). We aimed for SNRs per pixel of at least 100 near the 5500 Å wavelength region to maximize abundance precision. We summarize our observations in

[14] Note the lower SNR limit here. This is because there are insufficient M67 giants with SNR $>$ 300 APOGEE spectra.

Table 3
Sensitivity of Each Line's Derived Elemental Abundance ($\log \varepsilon(X)_\lambda$) in Response to Perturbing the Adopted Stellar Atmosphere by $\Delta T_{\rm eff} = 100$ K, $\Delta \log g = 0.10$, Δ[M/H] = 0.10, and $\Delta v_{\rm micro} = 0.1$ km s^{-1}

Element	Ion	Line (Å)	$\Delta \log \varepsilon(X)_\lambda$ given			
			$\Delta T_{\rm eff} = 100$ K	$\Delta \log g = 0.10$	Δ[M/H] = 0.10	$\Delta v_{\rm micro} = 0.10$ km s^{-1}
Na	1	4751.8	0.03	0.04	0.04	0.03
Ti	1	4758.1	0.07	0.03	0.08	0.12
Ti	1	4759.3	0.06	0.04	0.03	0.07
Ce	2	4773.9	0.03	0.06	0.06	0.03
…	…	…	…	…	…	…
Fe	1	5364.9	0.1	0.04	0.04	0.11
Fe	1	5365.4	0.08	0.04	0.08	0.18
Ti	1	5366.6	0.11	0.05	0.07	0.08
Fe	1	5379.6	0.08	0.03	0.04	0.11
Fe	1	5383.4	0.13	0.05	0.03	0.07
…	…	…	…	…	…	…
Fe	1	8621.6	0.09	0.06	0.01	0.15
Al	1	8773.9	0.11	0.02	0.03	0.05
Ti	1	8778.7	0.07	0.04	0.1	0.04
Fe	1	8846.7	0.02	0.03	0.03	0.05

Note. This table is used to assess the impact of stellar parameter uncertainties on final differential abundance uncertainties. While each element responds differently to changes in stellar parameters, the light, α, odd-Z, and Fe-peak elements are typically more sensitive to changes in $T_{\rm eff}$ while the neutron-capture elements are more sensitive to changes in log g.

(This table is available in its entirety in machine-readable form in the online article.)

Table 1. For simplicity, we refer to APOGEE doppelgängers by an arbitrary pair number, and each star in a pair is assigned a letter. "Pairs" 13 and 17 have four and three stars that qualify as doppelgängers, respectively. Pairs 29 and 44 also share a star (the "a" component of both).

To illustrate that our final sample consists of apparently unrelated field stars, we present their on-sky positions in Figure 1. Doppelgängers span a range of positions, on-sky separations, and parallaxes. No pairs appear to be comoving, as all have either large on-sky separations or significant differences in parallax, proper motion, and/or radial velocity. In Figure 2, we present a Kiel diagram for our sample of doppelgängers and M67 reference stars. The majority of our sample occupies the red clump, though a few pairs lie outside of the clump. Most stars have solar metallicity ([Fe/H] = 0 $\pm$ 0.02), though three pairs (Pairs 6, 49, and 211) have [Fe/H] ~ -0.10, Pair 47 has [Fe/H] $= -0.48$, and Pair 52, our lowest surface gravity pair, has [Fe/H] $= -0.58$.

We note that star "a" in Pair 15 possesses a resolved stellar companion that we only discovered during data acquisition, as it does not have enhanced RUWE and survived our cuts. K. El-Badry et al. (2021) reported that Pair 15a has a companion that is 4 magnitudes fainter and slightly bluer in color. Gaia reports a BP-RP color of 1.34 for the primary star and 0.98 for its companion. The companion appears to be a lower-mass main-sequence star, so it is unlikely that it donated mass to the primary star and affected its photospheric abundances. As such, we do not omit this pair from our study but do encourage caution when interpreting its abundances.

After acquisition, the raw Tull Coudé Spectrograph data are initially processed using the Tull Coudé Spectrograph Data Reduction Pipeline (TSDRP[15]). This pipeline performs essential calibration and extraction steps, including bias subtraction, trace identification, scattered light subtraction, wavelength calibration, flat-field correction, cosmic-ray rejection, and spectral extraction for each spectral order. Additionally, TSDRP provides deblazing, continuum normalization, and order combination to produce a single, fully processed spectrum. Radial velocities are determined for each spectrum using iSpec, and spectra are shifted to rest air wavelengths. Finally, subexposures of the same object are coadded by spline interpolating fluxes onto a shared wavelength grid and summing them together, weighing each flux array by the SNR of the subexposure. This method is more effective than median coadding when observing conditions (e.g., clouds, seeing) vary throughout the exposures (see discussion and treatment of this problem in D. W. Hogg & A. R. Casey 2024).

[15] https://github.com/grzeimann/TSDRP

3. Method

In this work, we require high abundance precision to enable the detection of potentially subtle chemical differences between pairs of stars. Precise stellar parameters are critical for achieving high abundance precision. Due to the high SNR of the APOGEE spectra (SNR $>$ 300 for the doppelgängers), APOGEE reports precise stellar parameters for our sample (mean $T_{\rm eff}$ and log g uncertainties of 8 K and 0.02 dex, respectively). Thus, we adopt APOGEE's $T_{\rm eff}$ and log g values and uncertainties for this work. Our analysis is entirely differential in nature, so precise differences in stellar parameters among stars are the priority. As such, concerns about global offsets between absolute APOGEE-reported stellar parameters and absolute stellar parameters derived from the optical (e.g., G. Nandakumar et al. 2022; V. Hegedűs et al. 2023) are not relevant in this differential context.

Though we adopt APOGEE $T_{\rm eff}$ and log g, we must still determine microturbulence ($v_{\rm micro}$) and spectral broadening

from our optical spectra. Though $v_{\rm micro}$ is reported by APOGEE, we find that adopting it for our spectra can lead to trends between the abundances of Fe I lines and their reduced equivalent widths. This can inflate the line-to-line abundance scatter and thus affect our abundance precision. As a result, we elect to measure our own $v_{\rm micro}$. We use BACCHUS (T. Masseron et al. 2016) to determine $v_{\rm micro}$, spectral broadening, and individual elemental abundances for our optical spectra. Additionally, we investigate whether APOGEE-reported $T_{\rm eff}$ and $\log g$ are consistent with results returned by BACCHUS using the Fe ionization-excitation method (see description in the next section). The results of this test are presented in the Appendix.

3.1. BACCHUS

We describe BACCHUS briefly in the following paragraphs and point readers to K. Hawkins et al. (2016), T. Nelson et al. (2021), C. R. Hayes et al. (2022), and the official manual[16] for a more detailed description. BACCHUS is a spectral synthesis and fitting tool designed for high-resolution data. It synthesizes spectra using the radiative transfer code TURBOSPECTRUM (B. Plez 2012) adopting the MARCS model atmosphere grid (B. Gustafsson et al. 2008) and assuming 1D local thermodynamic equilibrium (1D LTE). We adopt version 5 of the Gaia-ESO line-list for our atomic transition data (U. Heiter et al. 2021) and combine molecular transition data from numerous sources: CH from T. Masseron et al. (2014), C2, CN, OH, and MgH from T. Masseron (2025, private communication), SiH from R. L. Kurucz (1992), and TiO, FeH, and ZrO from B. Pelz (2025, private communication).

Stellar parameters for which BACCHUS can fit are $T_{\rm eff}$, $\log g$, [M/H], microturbulence ($v_{\rm micro}$), and spectral broadening, called the "convolution" parameter, which includes broadening due to instrumental resolution, macroturbulence, and projected stellar rotation. BACCHUS uses traditional Fe ionization-excitation balance to solve for stellar parameters in an iterative fashion. The process begins with the user's initial guess of the stellar parameters, which are used to interpolate over the MARCS grid and produce a starting model atmosphere. Initial abundances of individual Fe lines are determined by minimizing the χ^2 between the observed spectral line segment and an interpolation across five synthetic absorption lines with varying Fe abundance. Stellar parameters are then solved for simultaneously using an iterative process that adjusts the input model atmosphere in light of the last iteration's results. When solving for $v_{\rm micro}$ (the only parameter that we re-determine from the optical spectra), BACCHUS converges when there is a null trend between the abundances and reduced equivalent widths of Fe I lines. With BACCHUS, we obtain average $v_{\rm micro}$ uncertainties of 0.05 ± 0.02 km s^{-1}. To solve for the convolution parameter, BACCHUS iterates through possible values until it achieves an agreement between Fe line abundances determined using the line intensity and equivalent width methods (see the next paragraph).

With $T_{\rm eff}$, $\log g$, and [M/H] from APOGEE and $v_{\rm micro}$ and spectral broadening from BACCHUS, we determine abundances in 21 elements that span five nucleosynthetic families: the α (Mg, Ca, Si), odd-Z (Na, Al), Fe-peak (Fe, Sc, Ti, V, Cr, Co, Ni, Cu[17], Zn), slow neutron-capture process (Y, Zr, Ba, La, Ce), mixed (Nd), and rapid neutron-capture process (Eu) elements. We omit the light elements, as we lack access to reliable C, N, and O lines. BACCHUS uses four methods to determine a line's abundance: χ^2 minimization, synthetic equivalent widths, spectral synthesis, and line intensity. Each method starts in the same way. After interpolating across the MARCS model grid to obtain an atmosphere parameterized by the $T_{\rm eff}$, $\log g$, [M/H], microturbulence, and ($v_{\rm micro}$) determined or set in the previous step, five lines are synthesized: one line with the expected abundance assuming a solar abundance pattern scaled to the input model metallicity, and four additional lines with -0.6, -0.3, $+0.3$, and $+0.6$ dex relative to the expected abundance. The χ^2 method computes the χ^2 between the observed and five synthetic spectra and adopts the abundance that minimizes the polynomial fit to the χ^2 versus abundance trend. The equivalent width method measures the equivalent width of the five synthetic lines and uses interpolation to find the abundance that minimizes the difference between the synthetic and observed equivalent width. The spectral synthesis method is similar to χ^2 but instead finds the abundance solution that minimizes the difference between the synthetic and observed spectrum. Finally, the line intensity method is similar to the equivalent width method but considers line depth (the average flux of the five points nearest the line center) instead of equivalent width. The equivalent width and line intensity methods will only agree when a suitable spectral broadening parameter is assumed. When determining abundances, we only consider abundances from lines where all four methods return unflagged results (see description of flags in C. R. Hayes et al. 2022), and the χ^2 and equivalent width methods return consistent abundances within 0.1 dex. A list of all lines considered for abundance determination is presented in Table 2.

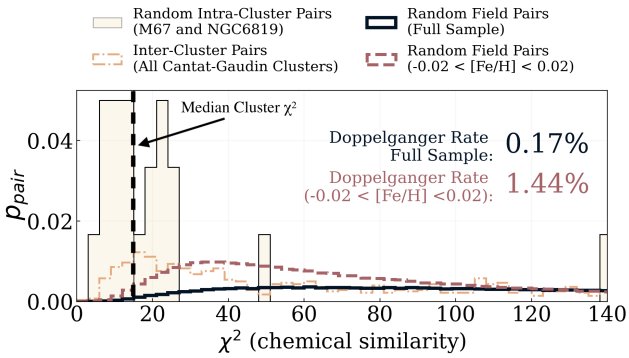

Figure 3. Shown here is our measurement of the APOGEE DR17 doppelgänger rate: defined as the rate at which randomly drawn pairs of field stars are as chemically similar as stars born together. This measurement is conducted by identifying the rate at which field stars possess χ^2 values (a metric of chemical similarity; see Equation (1)) less than or equal to the median χ^2 value of stellar pairs drawn from within open clusters. The solid black and dashed red curves present the distribution of χ^2 values for randomly drawn pairs of APOGEE field stars spanning the full [Fe/H] range and $-0.02 <$ [Fe/H] < 0.02, respectively. The χ^2 distribution for intracluster pairs is shown in yellow. As in N18, we also present the χ^2 distribution for intercluster (across different clusters) pairs with the orange dotted–dashed outline. Doppelgängers exist to the left of the median intracluster χ^2 value (vertical line). We measure a doppelgänger rate of 0.17% for the full DR17 sample and 1.44% for the narrow [Fe/H] range, comparable to similar measurements in DR13 and 16.

[16] BACCHUS Manual: https://drive.google.com/file/d/1VShSwA5M21q2pSSxLxc9AnoA19ixu-eV/view.

[17] Cu is also considered a neutron-capture element (e.g., M. Baratella et al. 2021).

Table 4
Mean Abundance Differences (Both Uncertainty Corrected and Uncorrected; See Section 4.2.1) and Mean Abundance Difference Uncertainties for the M67 and Doppelgänger Pairs

	M67			Doppelgängers		
El	Average Δ[X/Fe][a] (Corrected)	Average Δ[X/Fe][a] (Uncorrected)	Average Δ[X/Fe][a] Uncertainty	Average Δ[X/Fe][a] (Corrected)	Average Δ[X/Fe][a] (Uncorrected)	Average Δ[X/Fe][a] Uncertainty
Fe	0.018	0.018	0.006	0.017	0.017	0.006
Na	0.033	0.044	0.022	0.012	0.026	0.025
Mg	0.013	0.029	0.024	0.017	0.031	0.027
Al	0.005	0.014	0.012	0.013	0.022	0.012
Si	0.015	0.022	0.009	0.013	0.023	0.01
Ca	0.002	0.015	0.02	0.001	0.013	0.022
Sc	0.009	0.019	0.015	0.02	0.031	0.016
Ti	0.016	0.024	0.009	0.006	0.015	0.01
V	0.021	0.029	0.011	0.009	0.018	0.012
Cr	0.019	0.027	0.014	0.016	0.027	0.015
Co	0.005	0.015	0.013	0.012	0.021	0.015
Ni	0.007	0.018	0.016	0.009	0.019	0.017
Cu	0.0	0.018	0.039	0.007	0.022	0.043
Zn	0.016	0.052	0.082	0.004	0.040	0.090
Y	0.001	0.009	0.014	0.022	0.032	0.015
Zr	0.003	0.021	0.02	0.033	0.044	0.023
Ba	0.0	0.012	0.019	0.048	0.062	0.022
La	0.013	0.035	0.038	0.04	0.057	0.029
Ce	0.012	0.03	0.037	0.031	0.044	0.028
Nd	0.009	0.022	0.019	0.03	0.042	0.021
Eu	0.006	0.016	0.019	0.016	0.029	0.02

Note.
[a] Except for Fe, which is reported as [Fe/H].

3.1.1. Line-by-line Differential Abundance Analysis

To achieve high-precision abundances, we perform a line-by-line differential analysis to determine abundance differences among stars in doppelgänger or open cluster pairs. Line-by-line differential analysis is an effective way of minimizing abundance uncertainties and has been used widely for this purpose (again, e.g., J. Meléndez et al. 2012; D. Yong et al. 2013; J. Meléndez et al. 2014; M. Bedell et al. 2018; K. Hawkins et al. 2020; F. Liu et al. 2021; T. Nelson et al. 2021; D. Yong et al. 2023; F. Liu et al. 2024; and references in P. E. Nissen & B. Gustafsson 2018). In standard (nondifferential) abundance analysis, the abundance difference between two stars is determined in two steps: (1) adopting the final abundance of a star as the mean abundance derived from all well-measured lines, and (2) subtracting the final abundance of one star from another. This method is subject to sources of uncertainty that the line-by-line differential method bypasses. Due to poorly constrained log *gf*s[18] and systematics within the data reduction process (e.g., consistently underestimating the continuum near broad line regions, poorly addressing imperfections in certain regions of the CCD), lines of the same element across the same stellar spectrum will return inconsistent abundances. This inconsistency enlarges the final abundance uncertainty. In line-by-line differential abundance analysis, however, this line-to-line inconsistency becomes unimportant: abundance differences are measured independently for each individual line shared by both spectra, and the mean line-by-line abundance difference is adopted as the final abundance difference. In this way, uncertain log *gf*s and systematic imperfections in the data reduction process will affect both lines, and their impact will cancel out. See D. F. Gray (2008) for more on this effect.

In this work, each doppelgänger's abundance difference is determined by taking the average line-to-line abundance difference measured from all lines shared by the two stellar spectra, weighed by each line's differential abundance uncertainty. To determine each line's differential abundance uncertainty, we follow the formalism described in A. P. Ji et al. (2020). In short, we estimate the sensitivity of each line's measured abundance difference to changes in $\Delta T_{\rm eff}$, $\Delta \log g$, Δ[M/H], and $\Delta v_{\rm micro}$ among the two spectra using five representative doppelgänger pairs in our sample (Pairs 1, 13, 29, 49, and 52). This is accomplished by measuring the average line-by-line abundance differences among pairs where one star's $T_{\rm eff}$, $\log g$, [M/H], or $v_{\rm micro}$ was perturbed by 100 K, 0.1, 0.1, and 0.1 km s^{-1}, respectively. We present the average differential abundance sensitivities in Table 3. Note how different elements and lines show different sensitivities to changing stellar parameters. From here, we can derive empirical relationships between changes in $\Delta T_{\rm eff}$, $\Delta \log g$, Δ[M/H], or $\Delta v_{\rm micro}$ and $\Delta \log \varepsilon(X)_{\lambda}$, the abundance difference in line λ of element X. We apply these relationships to the stellar parameter uncertainties (again, using the method of A. P. Ji et al. 2020) to determine line-by-line differential abundance uncertainties. With differential abundance uncertainties estimated for each line, we can now estimate differential abundances and associated uncertainties for each element. Again, we do this by taking the average abundance difference across all lines of the element X weighted by the inverse variance of the individual differential abundance uncertainty of each line λ. As in A. P. Ji et al. (2020), the final adopted differential abundance uncertainty takes into account stellar parameter-driven differential

[18] The log *gf* of a line is the product of the statistical weight of the lower level of the transition (g) and the oscillator strength (f); see discussion in D. F. Gray (2008).

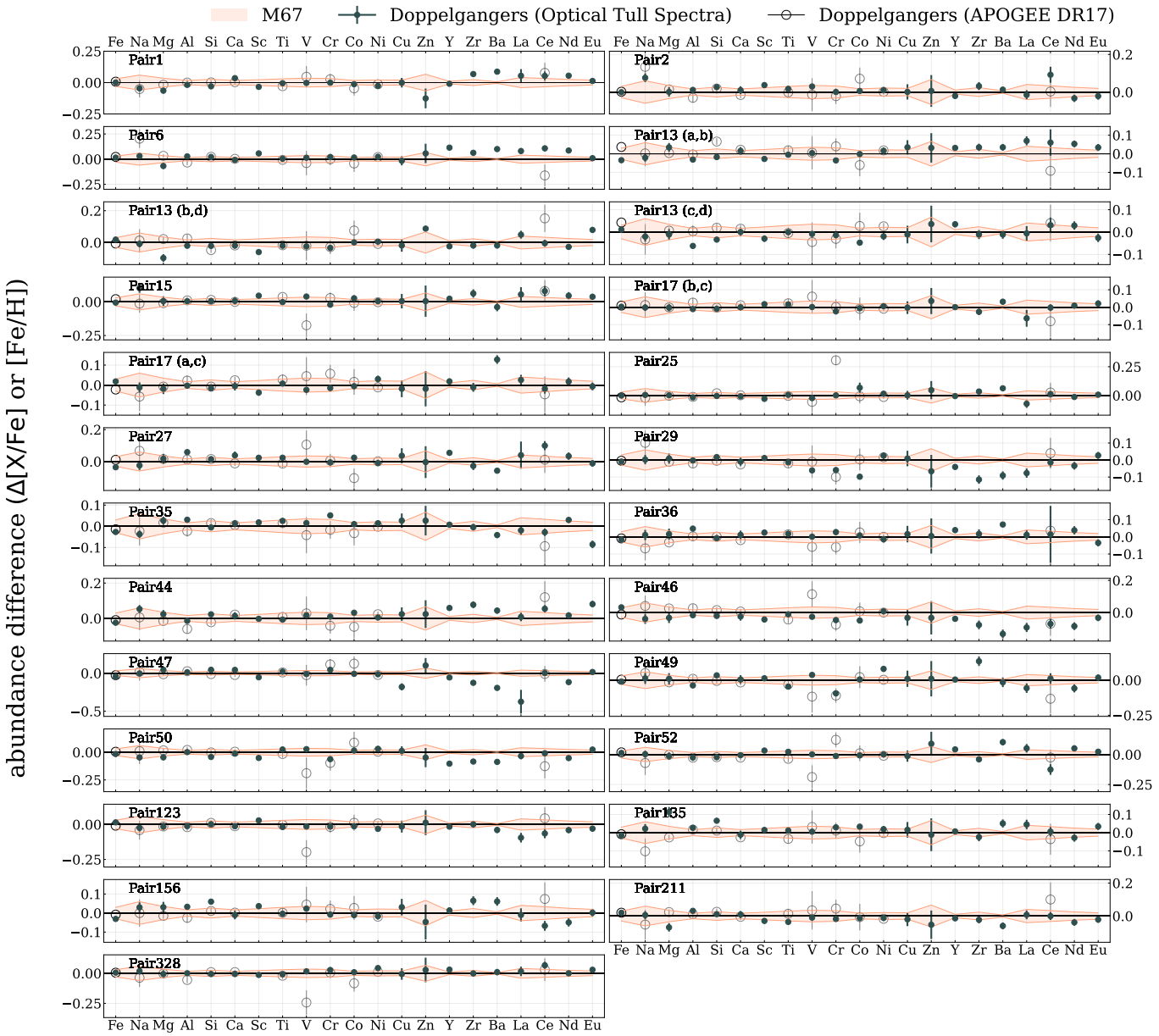

Figure 4. Differences in [X/Fe] (or, for Fe, [Fe/H]) for each APOGEE-identified chemical doppelgänger pair (filled circles) determined from our optical Tull spectra. Open circles indicate the equivalent APOGEE DR17-reported values where available. Orange fill indicates the standard deviation in abundance difference among M67 pairs. Doppelgängers are generally highly similar in the elements used in their initial selection (those with open circles that APOGEE can measure) but can differ significantly (beyond what is typical among M67 pairs) in the neutron-capture elements that APOGEE cannot access.

abundance uncertainties and the line-to-line differential abundance scatter.

4. Results

4.1. APOGEE DR17 Doppelgänger Rate

This work studies the chemical similarity of APOGEE-identified "chemical doppelgängers" from the optical, high-resolution point of view. To do this, we first identify doppelgängers for optical follow-up. In doing so, we conduct the first measurement of the APOGEE DR17 doppelgänger rate (Figure 3). The doppelgänger rate is a measure of the chemical diversity of stars in a population and places important constraints on Galactic chemical evolution. We find an APOGEE DR17 doppelgänger rate of 0.17% when considering the full high-fidelity APOGEE sample (see Section 2.1) and 1.44% for stars $-0.02 < [\mathrm{Fe/H}] < 0.02$. Both of these values agree well with previous measurements in DR13 (M. Ness et al. 2018) and DR 16 (D. de Mijolla et al. 2021). The median intracluster pairwise χ^2 value (see Equation (1)) is $\sim$15, just lower than the number of elements considered in computing the metric (17). This indicates that the reference open clusters (M67 and NGC 6819) are generally chemically homogeneous at or below the abundance uncertainty level in the elements considered according to APOGEE DR17.

4.2. Line-by-line Differential Abundances of Stellar Pairs

4.2.1. Chemical Homogeneity of Reference Open Cluster M67

According to our adopted definition, chemical doppelgängers are random pairs of disk stars that are as chemically similar as stars born together. To confirm the "doppelgänger"

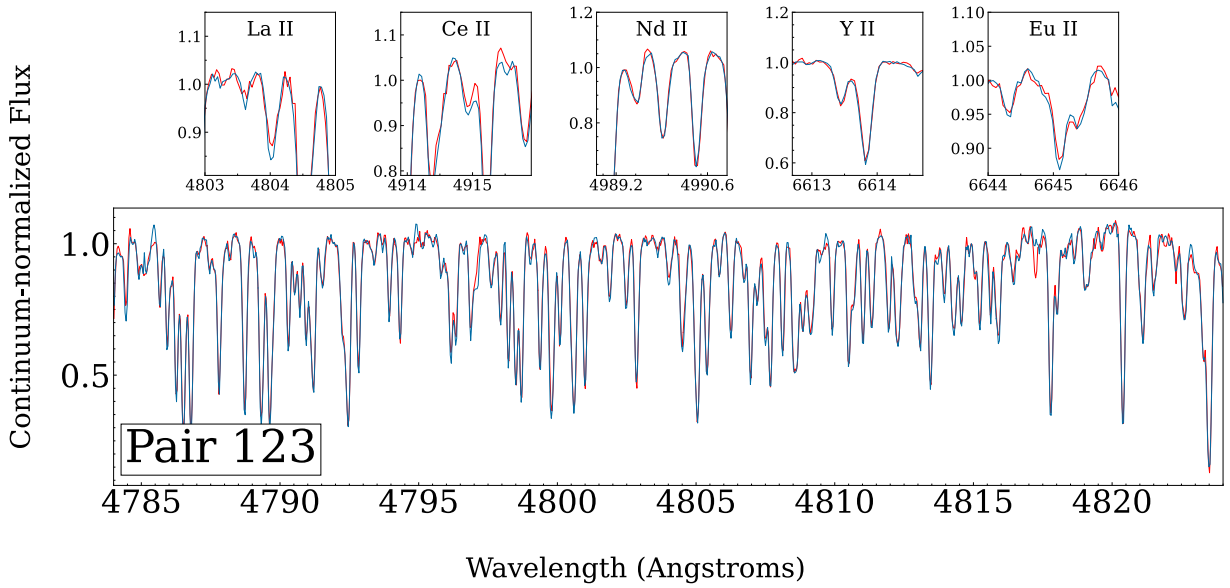

Figure 5. Tull spectra of the a (red) and b (blue) components of Pair 123. This pair differs detectably in [La/Fe] and [Ce/Fe] but not [Nd, Y, or Eu/Fe], and signs of this can be seen in the spectral zoom-ins at the top. In addition to these differences, doppelgängers generally share remarkably similar optical spectra.

status of our sample, we must first constrain the chemical similarity of stars born together. We pair our observed M67 stars into all unique combinations that satisfy the $T_{\rm eff}$ and log g similarity requirements of our initial doppelgänger selection ($\Delta T_{\rm eff} < 50$ K, $\Delta \log g < 0.1$ dex). This results in 24 unique open cluster pairs. We determine the average uncertainty-corrected abundance differences of these pairs (computed as the quadratic difference between the abundance difference and the associated uncertainty) and report them in Table 4. We find that M67 pairs on average differ by <0.02 dex (with the exception of Na, which shows an average abundance difference of 0.033) in [Fe/H] and [X/Fe], consistent with previous investigations of the cluster's chemical homogeneity (e.g., J. Bovy et al. 2016; M. Ness et al. 2018; A. Sinha et al. 2024; J. Kos et al. 2025).

4.2.2. *Differential Abundances of APOGEE-identified Chemical Doppelgängers*

With constraints on the abundance similarity of our reference M67 pairs, we can now assess the abundance similarities of our doppelgänger pairs. Given their selection, pairs should show small abundance differences comparable to those of the M67 pairs in the APOGEE-reported elements. We present the results of our line-by-line differential abundance analysis in Figure 4. According to our definition, stars are considered to be doppelgängers in an element when their abundance difference (filled circles) is less than the typical abundance differences among open cluster pairs. For this portion of our analysis, we use the standard deviation in the abundance differences among M67 pairs (orange fill) as a reference point. Our optical analysis confirms that APOGEE-identified chemical doppelgängers are indeed generally doppelgängers in the APOGEE-measured elements on which they were selected (Na through Fe in the periodic table). However, there are a few exceptions to this.

Pairs 2 and 15 show 0.08–0.10 dex [Na/Fe] differences that exceed the typical differences in M67 pairs. APOGEE also detects a significant [Na/Fe] difference in Pair 2 but with larger uncertainties. [Al/Fe] can also differ slightly (<0.03–0.06 dex) for several pairs (Pairs 13's c and d components, 27, 36, 49, and 156). These differences are small but significant because they are larger than the average for M67 pairs. [Mg/Fe] differs by 0.05–0.06 dex in Pairs 6, 13 (b and d), and 135, exceeding M67's 0.03 dex standard deviation in abundance difference. Si and Ca also differ subtly between pairs, with Pair 135 showing the largest difference (0.05 dex for Si). Several pairs (6, 13 b and d components, 15, 46, 47, and 50) show 0.04–0.06 dex differences in Sc but no other Fe-peak elements. Pair 328 shows a ∼0.07 dex difference in [Ni/Fe] but again no significant differences in the remaining Fe-peak elements. Pair 49 shows significant Ni and Cr differences but no such differences in other Fe-peak elements. Finally, Co differs slightly among Pairs 13 (c and d), 15, 46, and 135. Barring these exceptions, our optical analysis generally confirms the "doppelgänger" status of these stars in the lighter ($Z < 29$) elements on which they were selected, and our differential results agree well with APOGEE's.

Next, we will discuss the differential abundance results for the elements newly measured in the optical. Zn and Cu are elements either missing in or not well-measured by APOGEE and thus not used in the initial selection of doppelgängers. However, we can measure two Zn I lines (λ 4722.159, 4810.54 Å) up to four Cu I lines in our optical spectra (λ 5105.5, 5218.2,5220.1, and 5700.2 Å). Pairs 1, 13 (b and d), 47, and 52 show 0.09–0.13 dex differences in [Zn/Fe], though we highlight the significant 0.07 dex [Zn/Fe] spread in M67 for comparison and the 0.08 dex average abundance uncertainty). Pairs 27 and 47 are the only pairs to show significant (0.04 and 0.18 dex, respectively) differences in [Cu/Fe] compared to the 0.02 dex standard deviation among M67 pairs' abundance differences.

Finally, we can assess the neutron-capture (Zr, Y, La, Ce, Nd, and Eu) elemental abundance similarities of our doppelgänger sample. None of the 25 pairs can be considered doppelgängers in all neutron-capture elements. All doppelgängers show abundance differences in at least one neutron-capture element. Fifteen pairs show differences in one or both light *s*-process elements [Y/Fe] and [Zr/Fe] that exceed the

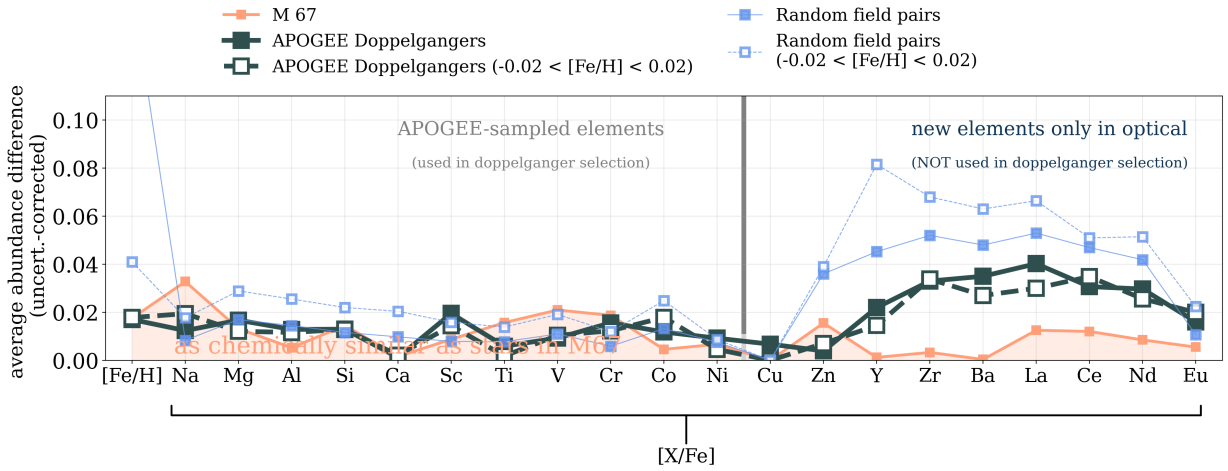

Figure 6. Average uncertainty-corrected abundance differences among all doppelgängers (filled dark-green squares) and just those with solar metallicity (open green squares). For comparison, we include the equivalent for M67 pairs (orange squares) and random, chemically unrelated field pairs (blue filled and open squares representing all and exclusively solar-metallicity field pairs). The position of the dark-green squares with respect to the orange ones indicates the distinguishing power of each element among APOGEE-identified chemical doppelgängers. This figure illustrates that Y, Zr, Ba, La, Ce, and Nd can typically distinguish between APOGEE-identified doppelgängers.

typical abundance spread within M67. Nineteen, 11, and 12 pairs differ significantly in heavy *s*-elements Ba, La, and Ce, respectively, beyond the typical difference among M67 pairs (up to 0.380 ± 0.150 dex for [La/Fe] in Pair 47). Mixed element Nd (see Section 5 for more on mixed elements) differs in 10 pairs. Finally, Eu differs significantly among five pairs (Pairs 13 b and d, 15, 35, 36, and 44).

There are instances where doppelgängers differ in a subset of the elements within a nucleosynthetic family but not the rest. For example, in Pair 123, the stars differ significantly in La and Ce but share indistinguishable compositions in the remaining neutron-capture elements. We visually inspect all doppelgänger spectra to confirm that abundance differences reflect line flux differences. We show an example comparison for Pair 123, whose spectra display generally indistinguishable Y, Nd, and Eu lines but flux differences around the La and Ce lines (Figure 5).

We summarize our differential analysis results in Figure 6, where we present the average uncertainty-corrected abundance differences among our doppelgänger pairs. Again, we define the uncertainty-corrected abundance difference to be the quadratic difference between the measured abundance and the associated uncertainty. This corrected form takes into account uncertainties and allows us to determine average abundance differences without adding scatter due to large uncertainties. To contextualize these differences, we compare them to the average uncertainty-corrected abundance differences among M67 pairs, a reference measure for the chemical similarity of stars born together. We also compare them to the opposite extreme, the chemical similarity of stars that were not born together, by determining the average uncertainty-corrected abundance differences among random field stars that are chemically unrelated. This comparison sample of random field pairs is created by recycling our doppelgänger sample but pairing stars randomly and excluding combinations of doppelgängers. We are unable to impose our strict $\Delta T_{\rm eff}$ and $\log g$ requirements for the random field pairs due to a lack of non-doppelgänger combinations that satisfy them, but we require that random pairs have $\Delta T_{\rm eff} < 100$ K and $\Delta \log g < 0.15$ dex. The standard deviation in Δ [X/Fe] for our doppelgänger sample captures the typical doppelgänger star-to-star difference in each element. When compared to the standard deviation of M67 pairs, this quantity also informs the distinguishing power of each element among APOGEE-identified chemically similar stars. For example, when doppelgängers' differential abundance spread in an element is less than or equal to that of M67 pairs, then the element does not typically distinguish APOGEE-identified chemical doppelgängers. When the typical abundance difference exceeds that of M67, this element can be used to distinguish between APOGEE-identified doppelgängers.

Figure 6 further confirms that in general, APOGEE-identified chemical doppelgängers indeed appear to be doppelgängers in the elements used to select them, though [Al, Si, and Sc/Fe] can differ slightly (<0.005 dex on average) among pairs beyond the typical differences found in M67 pairs. However, doppelgängers can show large abundance differences in the elements that APOGEE does not measure (or measures imprecisely). Our results suggest that APOGEE-identified doppelgängers can typically be distinguished by their differences in one or more *s*-process elements: the light *s*-process elements Y and Zr, the heavy *s*-process elements Ba, La, and Ce, and/or mixed element Nd. Within our sample of doppelgängers, Y, Zr, Ba, La, Ce, and Nd tend to differ by an amount 0.02–0.05 dex greater than that among M67 pairs. Interestingly, *r*-process element Eu shows comparatively smaller differences among doppelgängers, exceeding those of M67 pairs by 0.01 dex. [Eu/Fe] is thus less effective at distinguishing doppelgängers at the current precision of 0.02 dex. Furthermore, weak *s*-process elements Cu and Zn do not typically distinguish among doppelgängers.

4.3. Correlations between Chemical Similarity and Other Stellar Attributes

Our results so far have indicated that stars can appear to be chemically indistinguishable in APOGEE but differ significantly in some elements according to their high-resolution optical spectra. It is of interest to understand why some doppelgängers display abundance differences while others do not. Searching for relationships between doppelgängers'

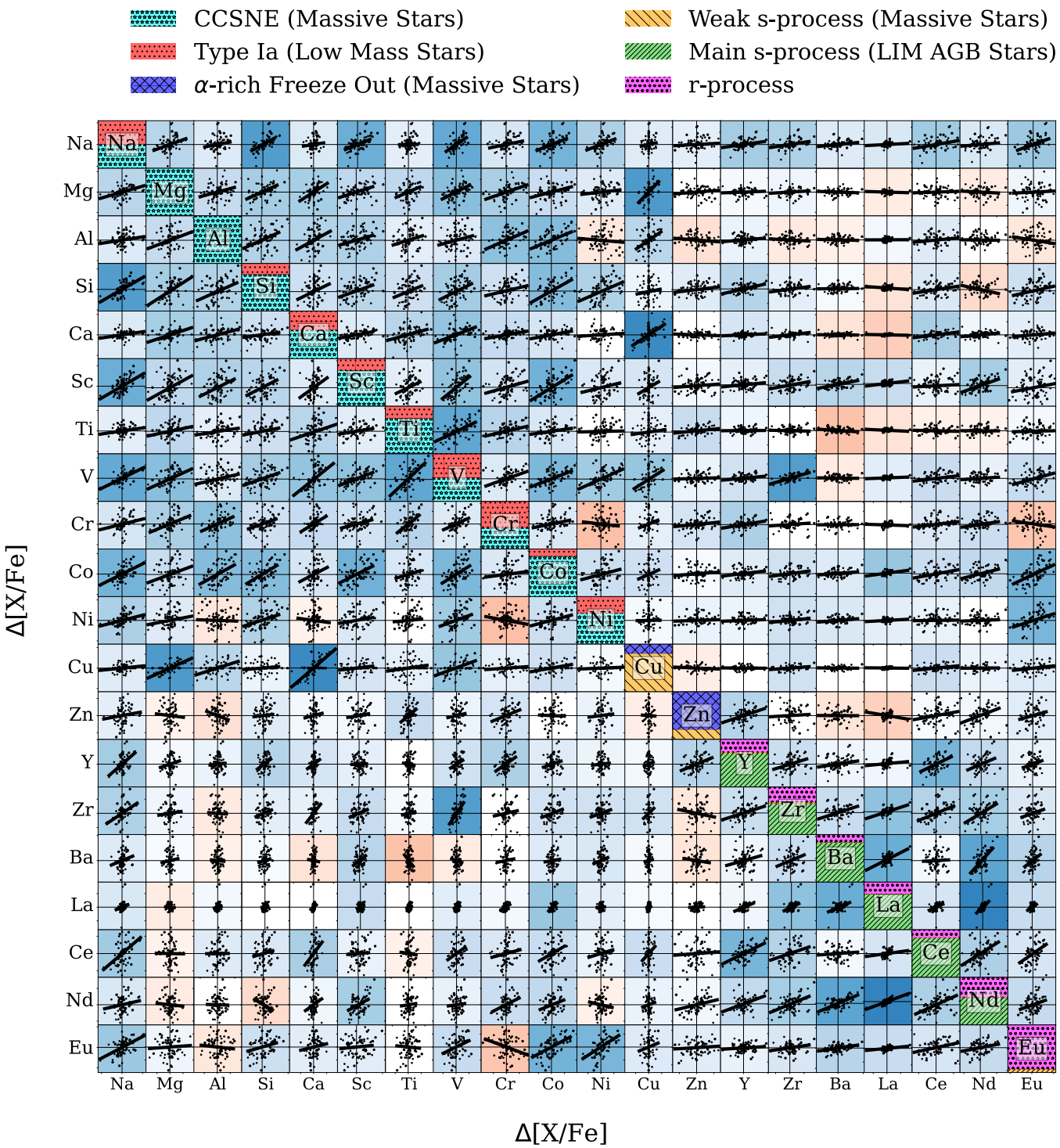

Figure 7. A comparison of doppelgängers' abundance difference (Δ[X/Fe]) in all combinations of elements measured in the optical spectra. In each panel, each pairs' abundance difference is reflected (shown twice) to illustrate the arbitrary ordering of the two stars. Lines represent the linear regression through the data in each grid-box; colors indicate the sign of the slope (blue for positive, red for negative); and transparency indicates the magnitude of the Pearson correlation coefficient. Diagonal elements are colored by relative contribution from various nucleosynthetic sources to the Sun's abundance in each element (S. Bisterzo et al. 2014; C. Kobayashi et al. 2020). Of the newly measured elements (Cu through Eu), heavy *s*-process elements Ba, La, Ce, and Nd show the strongest correlations with each other, indicating that stellar pairs (dis)similar in one of these elements tend to be (dis)similar in the others. (We use the Huber Regressor from scikit-learn, which is less influenced by outliers than other methods.)

abundance similarity and their similarity in other parameters may provide insights. Covariances between abundance similarity in elements produced through the same nucleosynthetic channel can validate our abundance determination method and provide insights into the nucleosynthetic origins of these abundance differences. For example, if doppelgängers that differ significantly in one element also differ consistently in others within the same nucleosynthetic family, then one could conclude that this nucleosynthetic channel is driving the variations.

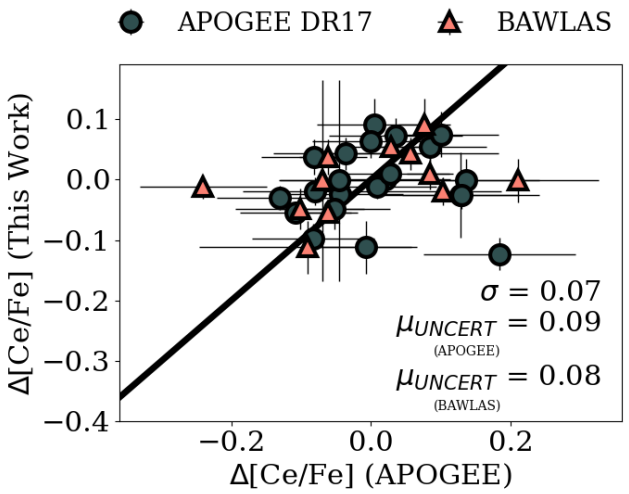

Figure 8. A comparison of this work's Δ[Ce/Fe] and those reported by APOGEE DR17 (navy circles) and BAWLAS (red triangles) for chemical doppelgängers in this sample. The one-to-one line is included in solid black. Our results generally agree within measurement uncertainties barring two exceptions. The Ce abundance uncertainties reported by APOGEE and BAWLAS exceed the median abundance differences between chemical doppelgängers measured in our optical analysis, hence why these stars were reported as doppelgängers in our initial search. However, our higher-precision optical analysis is able to distinguish between some doppelgängers using [Ce/Fe] and other neutron-capture elements.

Figure 7 compares doppelgängers' similarities in one element to those in other elements. Note that all points are reflected to illustrate the arbitrary ordering of stars in each pair. We find positive correlations between pairs' similarities in most light-, α, odd-Z, and Fe-peak elements. Though these abundance differences are small, correlations are still detected. Moving onto the newly measured elements, significant correlations exist between Cu, Mg, and Ca. We find strong correlations between heavy *s*-process elements Ba, La, Ce, and Nd, four elements that we found earlier can differ among doppelgängers (though Ce notably shows the weakest correlations with the other elements of the heavy *s*-process group). We find comparatively weaker correlations between light *s*-process elements Y and Zr and the rest of the *s*-process elements with the exception of Y and Ce. Correlations between light ($Z < 29$) and neutron-capture elements also exist. We see correlations between Zr and V and also weak ones between Eu, Co, and Ni.

4.4. [Ce/Fe] in APOGEE and BAWLAS

Our analysis suggests that highly chemically similar stars in APOGEE can show significant differences in the optically measured neutron-capture elements despite using APOGEE-reported Ce in our initial selection. This suggests that APOGEE-measured Ce may not be sufficient for distinguishing between stars that are otherwise chemically similar. To understand why this may be the case, we compare our optically measured pairwise Δ[Ce/Fe] to that reported by APOGEE and BAWLAS in Figure 8. Our measurements of Δ[Ce/Fe] generally agree with APOGEE's and BAWLAS's within uncertainties with a few exceptions. However, APOGEE's and BAWLAS's precisions in [Ce/Fe], which are on average 0.09 dex and 0.08 dex, respectively, exceed the typical neutron-capture element differences of our sample (<0.02–0.05 dex). Thus, compared to optically measured neutron-capture elements, APOGEE's and BAWLAS's [Ce/Fe] measurements are not sufficiently precise for resolving abundance differences that can exist among stars that are otherwise chemically indistinguishable in the lighter elements.

5. Discussion

5.1. Summary and Comparison to Prior Works

This work shows that APOGEE-DR17-identified "chemical doppelgängers" (see definition in Section 3) are not necessarily doppelgängers in the neutron-capture elements when studied in the optical at high resolution. In other words, there exist highly chemically similar disk stars that share nearly indistinguishable lighter ($Z < 29$) element abundances, nearly identical C/N ratios (a proxy for age in giants with similar stellar parameters; e.g., T. Spoo et al. 2022) but differ measurably in these elements. We emphasize that these differences are on average small (∼0.02–0.05 dex beyond the typical scatter in M67) but can reach over 0.20 and up to 0.38 dex. All 25 pairs have differences at this level in at least one neutron-capture element. This demonstrates that APOGEE DR17 abundances, even when measured for 17 elements from SNR > 300 spectra, are not always sufficient for identifying truly chemically similar stars in eight additional elements. That is, we find that the neutron-capture elements contribute additional information not captured by the lighter elements.

From a Galactic chemical evolution (GCE) point of view, these results demonstrate that the neutron-capture elements operate semi-independently from the lighter elements insofar as a giant star's lighter element abundances ($Z < 29$), including C and N, do not perfectly dictate its heavy element abundances. This semi-independence of the GCE of neutron-capture elements is supported by observations. For example, M. Bedell et al. (2018) performed a high-precision differential abundance analysis of solar twins in the solar neighborhood. Figure 3 of their work shows that at fixed stellar age, Sun-like stars in the solar neighborhood have a larger scatter in the abundances of Cu and neutron-capture elements than lighter elements. E. Griffith et al. (2025, in preparation) performed a similar study in the low-metallicity regime and also found that *s*-process elements show larger star-to-star scatter than the lighter elements. This suggests that in both the low- and solar-metallicity regimes, stars born at the same time can display a wider variety of Cu and neutron-capture element compositions than light element compositions. Furthermore, E. J. Griffith et al. (2022, 2024) showed that a two-process Galactic chemical evolution model described by relative contributions from Type Ia and Type II supernovae is not sufficient to predict the abundances of elements produced via the neutron-capture process. J. Mead et al. (2025) similarly found that the lighter elements cannot predict the neutron-capture elemental abundances of solar neighborhood stars beyond a precision of 0.02–0.05 dex, even when using abundances derived from high-SNR (SNR > 1000), high-resolution ($R \sim 110{,}000$) spectra. All of these results support the semi-independent GCE trajectories of these heavier elements. However, these amplitudes of 0.02–0.05 dex also represent the precision required on the measurements to access this independent information, which is otherwise obfuscated by noise.

5.2. Distinguishing Power of Individual Elements and Nucleosynthetic Channels

The distinct nucleosynthetic processes and sites that create the neutron-capture elements could explain why these elements are not perfectly traced by the lighter ones. The following subsections briefly review the nucleosynthetic origins of each element newly measured in this work and dissect our results on an element-by-element basis.

5.2.1. Weak S-process Elements: Copper and Zinc

Our optical analysis reveals that APOGEE DR17-identified chemical doppelgängers on average do not differ significantly in [Cu or Zn/Fe]. Their nucleosynthetic origins could provide an explanation. Though these elements (atomic numbers 29 and 30) are commonly associated with the Fe-peak group, their primary production mechanisms have been debated for decades (see discussion in E. Caffau et al. 2023). Cu was originally believed to be produced primarily via explosive nucleosynthesis in Type Ia and Type II supernovae (F. Matteucci et al. 1993). C. Sneden et al. (1991) were among the first to propose that the weak *s*-process in massive stars is the main source for the Sun's Cu abundance, and this was re-proposed by S. Bisterzo et al. (2005). Updates to neutron-capture reaction rates confirmed that in the metal-rich regime, Cu is primarily synthesized in massive stars ($M > 8\ M_{\odot}$) via the weak *s*-process M. Heil et al. (2008), and M. Pignatari et al. (2010) suggested that 70%–80% of Cu in the Sun was likely synthesized via this process. The weak *s*-process in massive stars operates during both the He core and C shell burning stages and produces elements between Fe and Mo (including Cu, Zn, Sr, Zr, and Y) in the periodic table. The free neutrons required for the weak *s*-process come from the ^{22}N(α, n)^{25}Mg reaction, which takes place primarily during the star's core He and C-burning phases (e.g., M. Pignatari et al. 2010; U. Frischknecht et al. 2016; M. Limongi & A. Chieffi 2018). Additionally, A. I. Karakas & M. Lugaro (e.g., 2016) found that Cu can also be synthesized in ∼solar-metallicity $M > 3M_{\odot}$ AGB stars via the *s*-process, though it is believed that only 5% of the Sun's Cu was produced in AGB stars (C. Travaglio et al. 2004; S. Bisterzo et al. 2005). Cu's primary dispersal mechanisms involve supernovae of various flavors, though it also enters the ISM via AGB winds. The element's primarily massive star origin leads it to show a strong [X/Fe] trend with stellar age in the solar neighborhood that mimics those of the alpha elements (e.g., L. Spina et al. 2016; M. Bedell et al. 2018).

The production site of Zn is similarly complicated (see Y. Hirai et al. 2018, and references therein). As for Cu, the weak *s*-process in massive stars produces Zn (e.g., S. E. Woosley & T. A. Weaver 1995). However, Zn is also produced in large quantities during alpha-rich freeze out, a process that occurs during the core-collapse explosion of a massive star. The Si-rich shell of the massive star is struck by the supernova shock, and its contents break down into alpha particles and other nucleons. When this material cools, the free alpha particles and nucleons reassemble into heavier elements including Zn (e.g., S. E. Woosley & T. A. Weaver 1995; G. C. Jordan et al. 2003). Finally, hypernovae (explosions with ∼1 dex greater kinetic energy than typical core-collapse supernovae) and electron-capture supernovae are also responsible for the Galactic reservoir of Zn (e.g., C. Kobayashi et al. 2006). In the Sun, alpha-rich freeze out is likely responsible for ∼80% of its Zn content, while the weak *s*-process is responsible for the remaining 20% (S. Bisterzo et al. 2014). Unlike in the case of Cu, Zn does not appear to be produced in AGB stars (A. I. Karakas & M. Lugaro 2016).

The unique nucleosynthetic origins of Cu and Zn, distinct from those of the light, α, and Fe-peak elements, make them potentially important elements for distinguishing among doppelgängers. However, evidently, doppelgängers on average do not differ in these elements. In the context of this work, elements produced primarily via the weak *s*-process in massive stars have no additional distinguishing power beyond the lighter elements. The shared dispersal mechanisms of Cu, Zn, and the lighter elements, namely supernovae, could be responsible (see discussion in Section 5.3.2 regarding implications for the mixing length of supernova products).

5.2.2. Light S-process Elements: Yttrium and Zirconium

Our results suggest that APOGEE-identified doppelgängers can differ significantly in [Y and Zr/Fe]. These elements are associated with the first *s*-process peak and referred to as light *s*-process (light *s*-) elements. Light *s*- elements are synthesized via both the weak *s*-process in massive stars (see discussion in previous subsection) and the main *s*-process in low- and intermediate-mass ($M < 8\ M_{\odot}$) AGB stars, where the required source of free neutrons comes from the ^{13}C(α, n)^{16}O reaction within the He-intershell (e.g., S. Cristallo et al. 2011; R. Longland et al. 2012; A. I. Karakas & M. Lugaro 2016; S. Cristallo et al. 2018). Products of the neutron-capture process are then dredged up to the surface before being expelled via its stellar wind. In AGB stars, neutron-capture nucleosynthesis and dredge up are part of a cyclical process that occurs during the thermally pulsing AGB phase. AGB stars can experience tens to hundreds of thermal pulses before neutron-capture nucleosynthesis ceases (e.g., A. I. Karakas & J. C. Lattanzio 2014). As with all neutron-capture elements, Y and Zr are not exclusively formed via the *s*-process and can also be synthesized via the *r*-process. Recent works estimate that 66% of Zr and 72% of Y in the solar system were formed via the *s*-process, respectively (S. Bisterzo et al. 2014; C. Kobayashi et al. 2020), with the rest synthesized via the *r*-process (see Section 5.2.5 discussing Eu). Despite belonging to the same nucleosynthetic group, Y and Zr behave differently in the Galactic disk. Though M. Bedell et al. (2018) showed that the [X/Fe] versus age trends for Y and Zr appear indistinguishable, Figure 11 in E. Delgado Mena et al. (2017) illustrates that [Zr/Fe] shows a strong inverse correlation with [Fe/H] while [Y/Fe] remains relatively constant. This could point to a greater contribution to Galactic [Zr/Fe] from massive stars.

Zr and Y differ on average by 0.035 dex, 0.02–0.03 dex greater than M67 pairs. As mentioned above, these elements have significant contributions from the main *s*-process in AGB stars, suggesting that this nucleosynthetic source could increase the chemical inhomogeneity of the disk.

5.2.3. Heavy S-process Elements: Lanthanum and Cerium

Ba, La, and Ce vary most significantly among APOGEE-identified chemical doppelgängers, on average by 0.03–0.048 dex and by over 0.25 dex for Pair 47. These elements are considered among the purest *s*-process elements with the lowest contributions from *r*-process nucleosynthetic sources.

Theoretical and observational works suggest that 85% of Ba, 76% of La, and 84% of Ce in the solar system was produced via the *s*-process, with the main *s*-process in low- and intermediate-mass AGB stars (see previous subsection) dominating production (e.g., C. Travaglio et al. 1999; N. Winckler et al. 2006; A. Serminato et al. 2009; S. Bisterzo et al. 2014; A. I. Karakas & J. C. Lattanzio 2014; C. Kobayashi et al. 2020). [Ba, La, and Ce/Fe] show the steepest gradients with stellar age in the solar neighborhood likely due to their low-mass AGB star origins (M. Bedell et al. 2018). The time delay between the production of Fe (which has significant contributions from high-mass, short-lived stars that end as Type II supernovae) and that of long-lived AGB stars causes steep abundance gradients with stellar age. This principle explains why heavy *s*- elements, when compared to pure Type II elements like Mg, are the strongest chemical clocks (e.g., B. Ratcliffe et al. 2024). Ba, La, Ce, and Y variations among doppelgängers indicate that AGB star nucleosynthesis likely plays a role in abundance variations among otherwise chemically indistinguishable stars.

5.2.4. Mixed Element: Neodymium

Our results show that Nd can sometimes distinguish between APOGEE-identified doppelgängers, on average showing differences 0.02 dex greater than those among M67 pairs. Nd is considered a mixed element, as it has significant contributions from both *s*- and *r*-process nucleosynthesis. In our solar system, 56% of Nd was produced through the *s*-process in low-mass AGB stars, while the rest was created through the *r*-process (S. Bisterzo et al. 2014; C. Kobayashi et al. 2020). See the next subsection for a discussion of the *r*-process and its astrophysical sources. Given our results for Y, Zr, Ba, La, and Ce, it is possible that Nd's AGB star contributions could be responsible for its enhanced distinguishing power.

5.2.5. r-process Element: Europium

This work finds that APOGEE-identified chemical doppelgängers can differ in [Eu/Fe] beyond abundance uncertainties 20% of the time. However, these differences are generally small, on average exceeding the abundance differences between pairs of M67 stars by just 0.01 dex.

Eu is the most accessible *r*-process element in solar-metallicity stellar spectra (e.g., S. Buder et al. 2024). The *r*-process is responsible for 94% of solar Eu (S. Bisterzo et al. 2014; C. Kobayashi et al. 2020), and there is significant debate surrounding its astrophysical sites. GCE trends for Eu suggest that *r*-process nucleosynthesis must be associated with both massive star evolution and neutron-star mergers (e.g., F. Matteucci et al. 2014; E. Delgado Mena et al. 2017; P. Saraf et al. 2023). Recently, observations of a gravitational-wave event generated by a neutron-star merger identified *r*-process elements in the optical spectrum, confirming the production of these elements through this channel (B. Côté et al. 2018). *r*-process elements have the greatest potential for stochastic variations among otherwise chemically similar field stars due to their nucleosynthetic sources being highly productive, energetic, and rare. Among our disk star sample, it appears that *r*-process products on average do not differ as significantly as *s*-process elements among otherwise chemically similar stars. However, they can still differentiate between one in five doppelgängers. Importantly, we find two pairs where [Eu/Fe] differs by up to 0.10 dex despite comparatively weaker *s*-process element differences. This result suggests that Eu can be considered as an additional, although typically less effective, dimension when identifying chemically (dis)similar disk stars, supporting previous work identifying [Eu/α] as an effective chemical tag (e.g., S. Monty et al. 2024).

Our results suggest that products of AGB star nucleosynthesis are most important for distinguishing among otherwise chemically similar disk stars. By contrast, Cu, Zn, and Eu, all elements that enter the ISM via supernovae, do not share this distinguishing power, although [Eu/Fe] can occasionally distinguish among pairs, something that could be attributed to the stochasticity of its production. The following two subsections present possible physical explanations for this phenomenon.

5.3. Possible Physical Interpretations

5.3.1. Possibility 1: High-resolution, Optically Measured Neutron-capture Elements May Provide Better Constraints on Stellar Age than APOGEE Abundances Alone

One possible explanation for why some APOGEE-identified doppelgängers differ in their *s*-process neutron-capture abundances despite sharing indistinguishable lighter element abundances could be rooted in the relationship between *s*-process elements and age. *s*-process elemental abundance ratios ([s/α] and [s/Al]) have been found to correlate strongly with stellar age, particularly in the solar neighborhood and outer Milky Way disk (e.g., G. Casali et al. 2020; J. Carbajo-Hijarrubia et al. 2024; B. Ratcliffe et al. 2024; G. Casali et al. 2025). It is therefore possible that doppelgängers with neutron-capture elemental abundance differences also differ in age.

Under this assumption, our results may demonstrate that *s*-process elemental abundances are better at identifying stars with similar ages than APOGEE DR17 abundances alone, even those measured from SNR $>$ 300 spectra. These results could indicate that [C/N] and [α/Fe], two chemical clocks available through APOGEE, are not as effective as [s/α or Al] at identifying coeval stars. While it has been shown that [α/Fe] is a weaker chemical clock (e.g., J. Carbajo-Hijarrubia et al. 2024) than [s/α], this has not been shown for [C/N] to our knowledge. The age–[C/N] relationship measured in T. Spoo et al. (2022), which was constrained using open clusters in APOGEE DR17, shows a comparable slope and scatter to that of the age–[s/α] trend measured in, e.g., B. Ratcliffe et al. (2024), which constrained the relationship using disk stars observed by GALAH. It has been shown, however, that the [C/N] chemical clock is unreliable in stars that experience extra mixing (e.g., M. Shetrone et al. 2019). It is possible that this extra mixing could affect the [C/N] ratios of some doppelgängers in our sample, and *s*-process elements, which do not suffer from this effect, are more reliable at tracing age in these cases.

If this explanation holds true, then it is possible that combining APOGEE abundances with GALAH- or Gaia-ESO-measured *s*-process elements (Zr, Y, Ba, La, Ce, and Nd) could better identify stars born at similar Galactic times than APOGEE abundances alone. These results suggest that when working with APOGEE abundances derived from SNR $>$ 300 spectra, *s*-process elemental abundance precisions of $\sim$0.02–0.050 dex would be most beneficial for resolving

typical neutron-capture abundance differences among APOGEE disk stars. Achieving such high precision is difficult without line-by-line differential analysis. Lower-precision abundances will still be helpful, though, as some doppelgängers in our sample differ by over 0.2 dex in *s*-process elements.

5.3.2. Possibility 2: High-resolution, Optically Measured Neutron-capture Elements May Provide Better Constraints on Galactic Birth Location than APOGEE Abundances Alone

While differences in stellar age could explain doppelgängers' differences in neutron-capture elements, it is also possible that age is not a factor. If we assume that APOGEE C/N is as precise an age indicator as [s/α or Al], as suggested by previous works (e.g., G. Casali et al. 2019; T. Spoo et al. 2022), and that stellar birth radius is traced by stellar age and metallicity (M. K. Ness et al. 2019; Y. Lu et al. 2022), then we can assume that the APOGEE-identified doppelgängers likely formed at the same time and Galactocentric birth radius. By studying the Cu, Zn, and neutron-capture elemental abundance differences among APOGEE doppelgängers, we are effectively exploring the behavior of these elements in roughly mono-age, mono-birth radius stellar populations. Under these assumptions, our results could indicate that neutron-capture elements show additional abundance variations in volumes of the ISM that are otherwise chemically homogeneous. This could indicate that similarity in neutron-capture elemental abundances may trace stars' similarity in Galactic birth location more finely than the lighter elements alone.

Adopting this framework, doppelgängers with similar *s*-process elemental abundances may have formed at more similar Galactocentric radii or more similar Galactocentric azimuths than doppelgängers that differ in their *s*-process elemental compositions. If azimuthal mixing of AGB star products is efficient, as suggested by some simulations (e.g., C. Zhang et al. 2025), then the former scenario is more likely. In this scenario, neutron-capture elements are well-mixed azimuthally but show greater variations radially (i.e., steeper radial gradients) in the ISM relative to the elements dispersed by supernovae. Evidence supporting this can be found in, e.g., M. Molero et al. (2023), which infers Galactic gradients of [La/H] and [Ce/H] up to 0.02 dex kpc^{-1} steeper than those of [Fe/H].

5.4. Optical Spectroscopy Complements H-band Spectroscopy

Our optical analysis suggests that APOGEE abundances do not tell a star's full nucleosynthetic story, even when SNR $>$ 300 spectra and [C/N] are available. Stars that APOGEE reports to be chemically indistinguishable can differ significantly in the elements with large *s*-process contributions (e.g., Y, Ba, La, Ce, and Nd). Evidently, this is true even when [Ce/Fe] measurements from the SNR $>$ 300 APOGEE spectra are available. At this SNR, [Ce/Fe] can be measured with an average precision of 0.08 dex from APOGEE spectra (Figure 8). However, according to our results, this exceeds the typical star-to-star Ce variations that APOGEE doppelgängers can display, so one cannot use APOGEE [Ce/Fe] to further distinguish between disk stars beyond what the lighter ($Z < 29$) elements already accomplish. This is further confirmed by testing the impact of including versus excluding [Ce/Fe] when measuring the APOGEE DR17 doppelgänger rate (a test we performed when creating Figure 3). There is no difference in the measured doppelgänger rate when including Ce.

Achieving the necessary neutron-capture element precision to further distinguish between stars is comparatively easier in the optical spectral regime where strong lines of the neutron-capture elements exist. For example, at comparable resolving power to APOGEE but one-third the SNR, one can measure [Ce/Fe] precisions between 0.03 and 0.05 dex in optical spectra (e.g., S. Buder et al. 2021; S. Randich et al. 2022), enough to distinguish between APOGEE-identified chemically similar stars. Furthermore, in the optical regime, several elements of the *s*-process family beyond Ce can be measured in tandem to further denoise the *s*-process signal of each star.

This work demonstrates that high-resolution, high-SNR optical spectroscopy of a small sample of stars can reveal important information about stellar nucleosynthesis and Galactic chemical evolution. Although surveys such as APOGEE/SDSS-V are observing millions of stars, much can be learned from a sample of just a few dozen with high-fidelity abundances (e.g., M. Bedell et al. 2018; L. Spina et al. 2018; J. Mead et al. 2025).

6. Conclusions

In this work, we assess the chemical similarity of APOGEE-identified "chemical doppelgängers" though the lens of optical, high-resolution spectroscopy. This point of view allows us to confirm their chemical similarity in the APOGEE-measured elements while also studying their abundances of Cu, Zn, and neutron-capture elements that are imprecisely (if at all) measured by the infrared survey. Our line-by-line differential analysis reveals that stars deemed by APOGEE DR17 to be chemical doppelgängers according to their light (C, N, O), α (Mg, Si, Ca), Fe-peak (Fe, Ni, Co, V, Sc, Cr), and odd-*Z* (Na, Al, S, K, Mn) elements can differ detectably in neutron-capture elements Zr, Y, Ba, La, Ce, Nd, and occasionally Eu. These differences range from Δ[X/Fe] $= 0.020 \pm 0.015$ to 0.380 ± 0.15 dex (4%–140%), and up to 0.05 dex (12%) on average. We find that doppelgängers that differ in one *s*-process element tend to differ in other *s*-process elements, though not always in equal magnitude. Additionally, we show that Ce measured from APOGEE spectra is not sufficient for resolving differences between otherwise chemically indistinguishable stars, but neutron-capture elements measured from optical, high-resolution spectra can resolve these differences. This work indicates that neutron-capture elements can aid in searches for chemically and (potentially) dynamically similar stars when used in tandem with the lighter ($Z < 29$) elements. Furthermore, our results suggest that even at fixed [C/N] and light element composition, stars can differ in neutron-capture elemental abundances. We discuss possible interpretations, which include imperfections with the [C/N] chemical clock that can be addressed with *s*-process-based chemical clocks and comparatively less efficient radial mixing of AGB star nucleosynthetic products.

Acknowledgments

The authors thank the reviewer for providing a careful review of this manuscript and helpful comments that improved the quality of this work. C.M. thanks Harriet Dinerstein, Adrian Price-Whelan, Adam Wheeler, Natalie Myers, Amaya Sinha, Laia Casamiquela, and David Weinberg for fruitful

discussions that enhanced the determination and interpretation of these results. C.M. thanks the Center for Computational Astrophysics' Astro Data, Nearby Universe, and Spectroscopy groups for faciliating group discussions that enhanced the interpretation of this work. C.M. thanks McDonald Observatory Staff Coyne Gibson, Phillip Macqueen, John Kuehne, Karen Sulewski, Patricia Granado, and Marcela Garcia for enabling this science by guiding, teaching, feeding, and housing C.M. as she gathered the observational data for this work. C.M. is supported by the NSF Astronomy and Astrophysics Fellowship award No. AST-2401638. K.H. is partially supported through the Wootton Center for Astrophysical Plasma Properties funded under the United States Department of Energy collaborative agreement DE-NA0003843. E.J.G. is supported by an NSF Astronomy and Astrophysics Postdoctoral Fellowship under award AST-2202135. K.V.J. is supported by Simons Foundation grant 1018465.

The following software and programming languages made this research possible: Python (version 3.9) and its packages astropy (Astropy Collaboration et al. 2013, 2018, 2022), scipy (P. Virtanen et al. 2020), matplotlib (J. D. Hunter 2007), pandas (version 0.20.2; The pandas development team 2020), and NumPy (S. van der Walt et al. 2011; C. R. Harris et al. 2020). This research has made use of the VizieR catalog access tool, CDS, Strasbourg, France. The original description of the VizieR service was published in A&AS 143, 23.

This work has made use of data from the European Space Agency (ESA) mission Gaia (https://www.cosmos. esa.int/gaia), processed by the Gaia Data Processing and Analysis Consortium (DPAC, https://www.cosmos.esa.int/web/gaia/dpac/consortium). Funding for the DPAC has been provided by national institutions, in particular the institutions participating in the Gaia Multilateral Agreement.

Appendix

In this work, we adopt APOGEE-reported $T_{\rm eff}$ and log g values because they are derived from SNR $>$ 300 spectra and exceed the precision we can achieve using BACCHUS on our optical spectra. However, it is of interest to check whether the APOGEE parameters satisfy Fe ionization-excitation balance —the method used by BACCHUS to determine these parameters. As this work is entirely differential, we check for the satisfaction of differential spectroscopic equilibrium (see, e.g., J. Meléndez et al. 2012; D. Yong et al. 2013; J. Meléndez et al. 2014; F. Liu et al. 2021; D. Yong et al. 2023; F. Liu et al. 2024, and references in P. E. Nissen & B. Gustafsson 2018), which requires a null trend between line-by-line Δ[Fe/H] versus excitation potential and an agreement between the average Δ[Fe I/H] and Δ[Fe II/H] values within 1σ.

The results of our investigation are presented in Figure 9. We find that in 13/25 pairs, Fe excitation balance is satisfied when adopting APOGEE's $T_{\rm eff}$. In an additional five pairs, Fe excitation balance would be satisfied within 0.005 dex eV^{-1}, which (according to empirical tests reported in the BACCHUS manual) requires a $<$25 K perturbation to $T_{\rm eff}$. In the remaining seven cases, APOGEE's $T_{\rm eff}$ does not satisfy excitation balance, and $T_{\rm eff}$ would need to be shifted by $>$25 K to satisfy it. These pairs are Pairs 13ab, 17ac, 35, 36, 44, 47, and 328. The most extreme case is Pair 35, which would require an adjustment of $\sim$130 K to satisfy excitation balance. The rest of the pairs would require an adjustment of 50 K. As for log g, we find that APOGEE's log g satisfies ionization balance for all pairs.

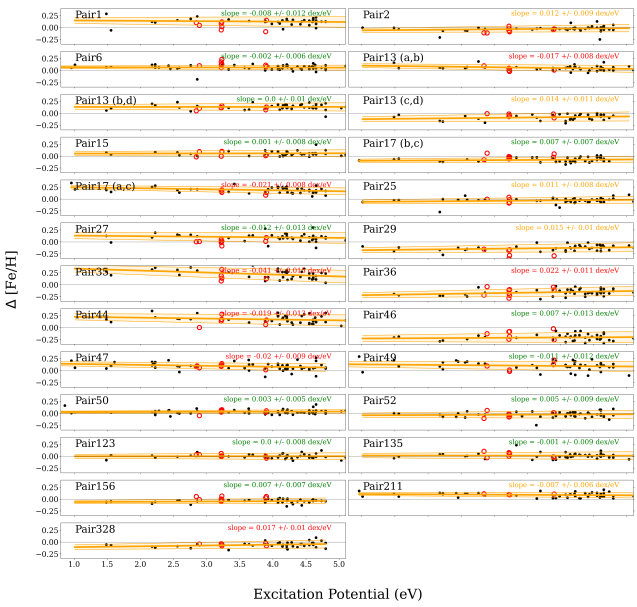

Figure 9. Line-by-line [Fe/H] differences among stars in each doppelgänger pair as a function of excitation potential determined from Fe I (black points) Fe II (red circles) absorption lines. The orange line and shaded region represent the best-fit line through the black points, and the slope and associated uncertainty in the slope are printed within each panel. If APOGEE-reported $T_{\rm eff}$ and log g differences satisfy Fe ionization-excitation balance, then the slope of each line should be consistent with zero, and average Δ[Fe/H] abundances of the black and red markers should agree within 1σ. When Fe excitation balance is satisfied (indicating suitable $T_{\rm eff}$), the text in the top right of each panel is colored green. Otherwise, it is orange (would be satisfied with a $<$25 K perturbation to $T_{\rm eff}$) or red (requires a larger perturbation of $T_{\rm eff}$).

This test indicates that APOGEE's parameters do not always satisfy Fe excitation equilibrium, indicating that the line-by-line Fe ionization-excitation method with BACCHUS would yield slightly different $T_{\rm eff}$ values for a subset of our sample. However, most importantly, we see no correlation between a lack of spectroscopic equilibrium satisfaction and the presence of significant s-process abundance differences, indicating that our results are not driven by the lack of excitation equilibrium. With the exception of Zr, our neutron-capture element abundances are determined from singly ionized lines, which are more sensitive to log g and ionization equilibrium. The slight $T_{\rm eff}$ perturbations that would be needed to satisfy excitation balance in a subset of the pairs would not impact our results for these elements. Furthermore, the ionization balance test has some limitations; it can have variable sensitivity and degeneracies between parameters as well as inherit systematics from 1D LTE model assumptions (e.g., P. Jofré et al. 2019). As such, it is not clear that parameters determined using the Fe ionization-excitation method on optical spectra would exceed the quality of those determined from APOGEE SNR $>$ 300 spectra.

ORCID iDs

Catherine Manea https://orcid.org/0000-0002-0900-6076
Melissa Ness https://orcid.org/0000-0001-5082-6693
Keith Hawkins https://orcid.org/0000-0002-1423-2174
Greg Zeimann https://orcid.org/0000-0003-2307-0629
David W. Hogg https://orcid.org/0000-0003-2866-9403

Carrie Filion https://orcid.org/0000-0001-5522-5029
Emily J. Griffith https://orcid.org/0000-0001-9345-9977
Kathryn Johnston https://orcid.org/0000-0001-6244-6727
Andrew Casey https://orcid.org/0000-0003-0174-0564
Zoe Hackshaw https://orcid.org/0000-0002-3855-3060
Tyler Nelson https://orcid.org/0000-0003-3707-5746

References

Abdurro'uf, A., Aerts, C., Silva Aguirre, V., et al. 2022, ApJS, 259, 35
Anders, F., Chiappini, C., Santiago, B. X., et al. 2014, A&A, 564, A115
Armillotta, L., Krumholz, M. R., & Fujimoto, Y. 2018, MNRAS, 481, 5000
Astropy Collaboration, et al. 2013, A&A, 558, A33
Astropy Collaboration, et al. 2018, AJ, 156, 123
Astropy Collaboration, et al. 2022, ApJ, 935, 167
Baratella, M., D'Orazi, V., Sheminova, V., et al. 2021, A&A, 653, A67
Bedell, M., Bean, J., Melendez, J., et al. 2018, ApJ, 865, 68
Belokurov, V., Erkal, D., Evans, N. W., Koposov, S. E., & Deason, A. J. 2018, MNRAS, 478, 611
Belokurov, V., Penoyre, Z., Oh, S., et al. 2020, MNRAS, 496, 1922
Bensby, T., Alves-Brito, A., Oey, M. S., Yong, D., & Meléndez, J. 2011, ApJL, 735, L46
Bisterzo, S., Pompeia, L., Gallino, R., et al. 2005, NuPhA, 758, 284
Bisterzo, S., Travaglio, C., Gallino, R., Wiescher, M., & Käppeler, F. 2014, ApJ, 787, 10
Bland-Hawthorn, J., Krumholz, M. R., & Freeman, K. 2010, ApJ, 713, 166
Bovy, J. 2016, ApJ, 817, 49
Bovy, J., Bahmanyar, A., Fritz, T. K., & Kallivayalil, N. 2016, ApJ, 833, 31
Bovy, J., Rix, H.-W., Liu, C., et al. 2012, ApJ, 753, 148
Buck, T. 2020, MNRAS, 491, 5435
Buder, S., Asplund, M., Duong, L., et al. 2018, MNRAS, 478, 4513
Buder, S., Sharma, S., Kos, J., et al. 2021, MNRAS, 506, 150
Buder, S., Kos, J., Wang, X. E., et al. 2025, PASA, 42, e051
Caffau, E., et al. 2023, MNRAS, 518, 3796
Cantat-Gaudin, T., Jordi, C., Vallenari, A., et al. 2018, A&A, 618, A93
Carbajo-Hijarrubia, J., Casamiquela, L., Carrera, R., et al. 2024, A&A, 687, A239
Carrillo, A., Deason, A. J., Fattahi, A., Callingham, T. M., & Grand, R. J. J. 2024, MNRAS, 527, 2165
Carrillo, A., Hawkins, K., Jofré, P., et al. 2022, MNRAS, 513, 1557
Casali, G., Magrini, L., Tognelli, E., et al. 2019, A&A, 629, A62
Casali, G., Spina, L., Magrini, L., et al. 2020, A&A, 639, A127
Casali, G., Montalban, J., Miglio, A., et al. 2025, MNRAS, 541, 2631
Casamiquela, L., Soubiran, C., Jofre, P., et al. 2021, A&A, 652, A25
Cheng, C. M., Price-Jones, N., & Bovy, J. 2021, MNRAS, 506, 5573
Ciucă, I., Kawata, D., Ting, Y. -S., et al. 2024, MNRAS, 528, L122
Côté, B., Fryer, C. L., Belczynski, K., et al. 2018, ApJ, 855, 99
Côté, B., Belczynski, K., Fryer, C. L., et al. 2017, ApJ, 836, 230
Cristallo, S., Piersanti, L., Straniero, O., et al. 2011, ApJS, 197, 17
Cristallo, S., La Cognata, M., Massimi, C., et al. 2018, ApJ, 859, 105
Cunha, K., Smith, V. V., Hasselquist, S., et al. 2017, ApJ, 844, 145
de Mijolla, D., Ness, M., Viti, S., & Wheeler, A. 2021, ApJ, 913, 12
Delgado Mena, E., Adibekyan, T. M., Sousa, V. Z., et al. 2017, A&A, 606, A94
El-Badry, K., Rix, H.-W., & Heintz, T. M. 2021, MNRAS, 506, 2269
Emerick, A., Bryan, G. L., & Mac Low, M.-M. 2020, ApJ, 890, 155
Feng, Y., & Krumholz, M. R. 2014, Natur, 513, 523
Feuillet, D. K., Feltzing, S., Sahlholdt, C., & Bensby, T. 2022, ApJ, 934, 21
Foster, S., Schiavon, R. P., de Castro, D. B., et al. 2024, A&A, 689, A230
Freeman, K., & Bland-Hawthorn, J. 2002, ARA&A, 40, 487
Frischknecht, U., Hirschi, R., Pignatari, M., et al. 2016, MNRAS, 456, 1803
Fuhrmann, K. 1998, A&A, 338, 161
Gilmore, G., Randich, S., Worley, C. C., et al. 2022, A&A, 666, A120
Gratton, R., Carretta, E., Matteucci, F., & Sneden, C. 1996, in ASP Conf. Ser. 92, Formation of the Galactic Halo...Inside and Out., ed. H. L. Morrison & A. Sarajedini (San Francisco, CA: ASP), 307
Gray, D. F. 2008, The Observation and Analysis of Stellar Photospheres (Cambridge: Cambridge Univ. Press)
Griffith, E. J., Hogg, D. W., Hasselquist, S., et al. 2025, AJ, 169, 280
Griffith, E. J., Weinberg, D. H., Buder, S., et al. 2022, ApJ, 931, 23
Gustafsson, B., Edvardsson, B., Eriksson, K., et al. 2008, A&A, 486, 951
Harris, C. R., Millman, K. J., van der Walt, S. J., et al. 2020, Natur, 85, 357
Hasselquist, S., Shetrone, M., Cunha, K., et al. 2016, ApJ, 833, 81
Hawkins, K., Lucey, M., Ting, Y. -S., et al. 2020, MNRAS, 492, 1164
Hawkins, K., Masseron, T., Jofré, P., et al. 2016, A&A, 594, A43
Hayden, M. R., Bovy, J., Holtzmann, J. A., et al. 2015, ApJ, 808, 132
Hayes, C. R., Majewski, S. R., Shetrone, M., et al. 2018, ApJ, 852, 49
Hayes, C. R., Masseron, T., Sobeck, J., et al. 2022, ApJS, 262, 34
Haywood, M., Di Matteo, P., Lehnert, M. D., et al. 2018, ApJ, 863, 113
Hegedűs, V., Mészáros, S., Jofré, P., et al. 2023, A&A, 670, A107
Heil, M., Käppeler, F., Uberseder, E., Gallino, R., & Pignatari, M. 2008, PhRvC, 77, 015808
Heiter, U., Lind, K., Bergemann, M., et al. 2021, A&A, 645, A106
Helmi, A., Babusiaux, C., Koppelman, H. H., et al. 2018, Natur, 563, 85
Hirai, Y., Saitoh, T. R., Ishimaru, Y., & Wanajo, S. 2018, ApJ, 855, 63
Hogg, D. W., & Casey, A. R. 2024, arXiv:2403.11011
Horta, D., Price-Whelan, A. M., Hogg, D. W., et al. 2024, ApJ, 962, 165
Hunter, J. D. 2007, CSE, 9, 90
Imig, J., Price, C., Holtzman, J. A., et al. 2023, ApJ, 954, 124
Ji, A. P., Li, T. S., Simon, J. D., et al. 2020, ApJ, 889, 27
Jofré, P., Heiter, U., & Soubiran, C. 2019, ARA&A, 57, 571
Jordan, G. C., Gupta, S. S., & Meyer, B. S. 2003, PhRvC, 68, 065801
Karakas, A. I., & Lattanzio, J. C. 2014, PASA, 31, e030
Karakas, A. I., & Lugaro, M. 2016, ApJ, 825, 26
Kobayashi, C., Karakas, A. I., & Lugaro, M. 2020, ApJ, 900, 179
Kobayashi, C., Umeda, H., Nomoto, K., Tominaga, N., & Ohkubo, T. 2006, ApJ, 653, 1145
Kos, J., Bland-Hawthorn, J., Buder, S., et al. 2021, MNRAS, 506, 4232
Kos, J., Buder, S., Beeson, K. L., et al. 2025, arXiv:2501.06140
Krumholz, M. R., & Ting, Y.-S. 2018, MNRAS, 475, 2236
Kurucz, R. L. 1992, in IAU Symp. 149, The Stellar Populations of Galaxies, ed. B. Barbuy & A. Renzini (Dordrecht: Kluwer), 225
Lian, J., Zasowski, G., Mackereth, T., et al. 2022, MNRAS, 513, 4130
Limongi, M., & Chieffi, A. 2018, ApJS, 237, 13
Liu, F., Asplund, M., Yong, D., et al. 2016, MNRAS, 463, 696
Liu, C., Fu, J., Shi, J., et al. 2020, arXiv:2005.07210
Liu, F., Ting, Y. -S., Yong, D., et al. 2024, Natur, 627, 501
Liu, F., Bitsch, B., Asplund, M., et al. 2021, MNRAS, 08, 1227
Longland, R., Iliadis, C., & Karakas, A. I. 2012, PhRvC, 85, 065809
Lu, Y., Buck, T., Minchev, I., & Ness, M. K. 2022, MNRAS, 515, L34
Majewski, S. R., Schiavon, R. P., Frinchaboy, P. M., et al. 2017, AJ, 154, 94
Manea, C., Hawkins, K., Ness, M. K., et al. 2024, ApJ, 972, 69
Masseron, T., Plez, B., Van Eck, S., et al. 2014, A&A, 571, A47
Masseron, T., Merle, T., & Hawkins, K., 2016 BACCHUS: Brussels Automatic Code for Characterizing High Accuracy Spectra, Astrophysics Source Code Library, ascl:1605.004
Matteucci, F., Raiteri, C. M., Busson, M., Gallino, R., & Gratton, R. 1993, A&A, 272, 421
Matteucci, F., Romano, D., Arcones, A., Korobkin, O., & Rosswog, S. 2014, MNRAS, 438, 2177
Mead, J., De La Garza, R., & Ness, M. 2025, arXiv:2504.18532
Meléndez, J., Bergemann, M., Cohen, J. G., et al. 2012, A&A, 543, A29
Meléndez, J., Schirbel, L., Monroe, T. R., et al. 2014, A&A, 567, L3
Molero, M., Magrini, L., Matteucci, F., et al. 2023, MNRAS, 523, 2974
Monty, S., Belokurov, V., Sanders, J., et al. 2024, MNRAS, 533, 2420
Nandakumar, G., Hayden, M. R., Sharma, S., et al. 2022, MNRAS, 513, 232
Nelson, T., Ting, Y.-S., Hawkins, K., et al. 2021, ApJ, 21, 118
Ness, M., Hogg, D. W., Rix, H. W., Ho, A. Y. Q., & Zasowski, G. 2015, ApJ, 808, 16
Ness, M., Rix, H. -W., Hogg, D. W., et al. 2018, ApJ, 853, 198
Ness, M. K., Johnston, K. V., Blancato, K., et al. 2019, ApJ, 883, 177
Nissen, P. E. 2015, A&A, 579, A52
Nissen, P. E., & Gustafsson, B. 2018, A&ARv, 6, 6
Ortigoza-Urdaneta, M., Vieira, K., Fernandez-Trincado, J. G., et al. 2023, A&A, 676, A140
Pignatari, M., Gallino, R., Heil, M., et al. 2010, ApJ, 710, 1557
Plez, B., 2012 Turbospectrum: Code for Spectral Synthesis, Astrophysics Source Code Library, ascl:1205.004
Poovelil, V. J., Zasowski, G., Hasselquist, S., et al. 2020, ApJ, 903, 55
Price-Jones, N., Bovy, J., Webb, J. J., et al. 2020, MNRAS, 496, 5101
Price-Whelan, A. M., Hogg, D. W., Johnston, K. V., et al. 2021, ApJ, 910, 17
Randich, S., Gilmore, G., Magrini, L., et al. 2022, A&A, 666, A121
Ratcliffe, B., Minchev, I., Cescutti, G., et al. 2024, MNRAS, 528, 3464
Re Fiorentin, P., Spagna, A., Lattanzi, M. G., & Cignoni, M. 2021, ApJL, 907, L16
The pandas development team 2020, pandas-dev/pandas: Pandas, v2.3.2, Zenodo, doi:10.5281/zenodo.3509134
Recio-Blanco, A., Fernández-Alvar, E., de Laverny, P., et al. 2021, A&A, 648, A108
Reddy, B. E., Tomkin, J., Lambert, D. L., & Allende Prieto, C. 2003, MNRAS, 340, 304

Roman, N. G. 1952, ApJ, 116, 122
Saraf, P., Prieto, C. A., Sivarani, T., et al. 2023, MNRAS, 524, 5607
Serminato, A., Gallino, R., Travaglio, C., Bisterzo, S., & Straniero, O. 2009, PASA, 26, 153
Shetrone, M., Tayar, J., Johnson, J. A., et al. 2019, ApJ, 872, 137
Simmerer, J., Sneden, C., Cowan, J. J., et al. 2004, ApJ, 617, 1091
Sinha, A., Zasowski, G., Frinchaboy, P., et al. 2024, ApJ, 975, 89
Sneden, C., Gratton, R. G., & Crocker, D. A. 1991, A&A, 246, 354
Souto, D., Cunha, K., Smith, V. V., et al. 2018, ApJ, 857, 14
Souto, D., Allende Prieto, C., Cunha, K., et al. 2019, ApJ, 874, 97
Spina, L., et al. 2018, MNRAS, 474, 2580
Spina, L., Magrini, L., Sacco, G. G., et al. 2022, A&A, 668, A16
Spina, L., Meléndez, J., Karakas, A. I., et al. 2016, A&A, 593, A125
Spoo, T., Tayar, J., Frinchaboy, P., et al. 2022, AAS Meeting, 240, 201.05
Sun, W. X., Huang, Y., Wang, H. -F., et al. 2020, ApJ, 903, 12
Tinsley, B. M. 1968, ApJ, 151, 547
Tinsley, B. M. 1979, ApJ, 229, 1046
Travaglio, C., Galli, D., Gallino, R., et al. 1999, ApJ, 521, 691
Travaglio, C., Gallino, R., Arnone, E., et al. 2004, ApJ, 601, 864
Tull, R. G., MacQueen, P. J., Sneden, C., & Lambert, D. L. 1995, PASP, 107, 251
van der Walt, S., Colbert, S. C., & Varoquaux, G. 2011, CSE, 13, 22
Vincenzo, F., Spitoni, E., Calura, F., et al. 2019, MNRAS, 487, L47
Virtanen, P., Gommers, R., Oliphant, T. E., et al. 2020, NatMe, 17, 261
Vitali, S., Slumstrup, D., Jofré, P., et al. 2024, A&A, 687, A164
Wallerstein, G. 1962, ApJS, 6, 407
Winckler, N., Dababneh, S., Heil, M., et al. 2006, ApJ, 647, 685
Woosley, S. E., & Weaver, T. A. 1995, ApJS, 101, 181
Yong, D., Melendez, J., Grundahl, F., et al. 2013, MNRAS, 34, 3542
Yong, D., Liu, F., Ting, Y., et al. 2023, MNRAS, 526, 2181
Zhang, C., Li, Z., Hu, Z., & Krumholz, M. R. 2025, MNRAS, 540, 3906